Stability and Structure of Stretched Vortices

Thesis by

Aurelius Prochazka

In Partial Fulfillment of the Requirements

for the Degree of

Doctor of Philosophy

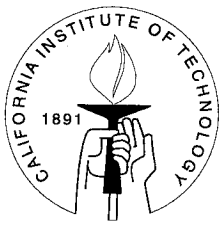

California Institute of Technology

Pasadena, California

1997

(Submitted January 17, 1997)

Acknowledgements

I thank my advisor, Professor Dale I. Pullin, for his guidance during each phase of the development of this thesis. I have found his ability to tailor his advising style to best engage each of his students to be truly remarkable, and I am grateful for all of his wise advice. Of course, I am very grateful for the support he has given me as well as the partial support provided by the National Science Foundation.

Helpful discussions with Professor Philip G. Saffman, James Buntine, Ron Henderson, and Darren Crowdy, are gratefully acknowledged. Thanks to Eve Andersson and Ashish Misra for assisting me with the seminar talk preparation. In addition to Dr. Pullin and Dr. Saffman, I thank the remaining members of my committee, Professors Hans G. Hornung, Tony Leonard, and David M. Grether.

Special attention must be brought to David Hill, who has helped me with many applied math concepts that played an important part in the development of my research. Perhaps more importantly, Dave's friendship and wit helped make my years at Caltech very enjoyable.

Finally, I thank my mother for her constant love and support and I dedicate this thesis to my grandfather, Vlad Stepanik.

Abstract

We investigate, numerically and analytically, the structure and stability of steady and quasi-steady solutions of the Navier-Stokes equations corresponding to steady stretched vortices embedded in a uniform nonsymmetric straining field, $(\alpha x, \beta y, \gamma z)$, $\alpha + \beta + \gamma = 0$, one principal axis of extensional strain of which is aligned with the vorticity. These are known as nonsymmetric Burgers vortices studied first by Robinson and Saffman (1984). We consider vortex Reynolds numbers $R = \Gamma/(2\pi\nu)$ where Γ is the vortex circulation and ν the kinematic vorticity, in the range Re = 1-10^4, and a broad range of strain ratios $\lambda = (\beta - \alpha)/(\beta + \alpha)$ including $\lambda > 1$, and in some cases $\lambda \gg 1$. A pseudo-spectral method is used to obtain numerical solutions corresponding to steady vortex states over our whole (R-λ) parameter space including $\lambda > 1$, where arguments proposed by Moffatt, Kida, and Ohkitani (1994) suggest the nonexistence of steady solutions. When $\lambda \gg 1$, $R \gg 1$ and $\varepsilon \equiv \lambda/R \ll 1$, we find an accurate asymptotic form for the vorticity in a region $1 < r/\sqrt{2\nu/\gamma} \leq \varepsilon^{-1/2}$, giving, in some cases, near machine-precision agreement with our numerical solutions. This suggests the existence of an extended region where the exponentially small vorticity is confined to a near cat's-eye shaped region of the almost two-dimensional flow, and takes a constant value nearly equal to $\Gamma\gamma/(4\pi\nu)\exp[-1/(2e\varepsilon)]$ on bounding streamlines. This allows an estimate of the leakage rate of circulation to infinity as $\partial\Gamma/\partial t = (.48475/4\pi)\gamma\varepsilon^{-1}\Gamma\exp(-1/2e\varepsilon)$ with corresponding exponentially slow decay of the vortex when $\lambda > 1$. This leakage rate differs substantially from that estimated by Moffatt, Kida, and Ohkitani. The normal-mode linear stability of the axisymmetric Burgers vortex ($\lambda = 0$) to two-dimensional disturbances is calculated in detail and the vortex is found to be stable at all Reynolds numbers. An iterative technique based on the Power method is used to estimate the largest eigenvalues for the nonsymmetric case $\lambda > 0$. Stability is found for $0 \leq \lambda \leq 1$, and a neutrally convective mode of instability is found and analyzed analytically for $\lambda > 1$. Our general con-

clusion is that the generalized nonsymmetric Burgers vortex is unconditionally stable to two-dimensional disturbances for all R, $0 \leq \lambda \leq 1$, and that the vortex will tend to move with the background strain when $\lambda > 1$, but maintain its structure which will change only through exponentially slow leakage of vorticity, indicating extreme robustness in this case.

Contents

List of Figures

List of Tables

Chapter 1 Introduction and Motivation

1.1 Burgers vortex

Two important dynamical mechanisms active in the fine scales of turbulence are known to be the intensification of vorticity through vortex stretching and the dissipation of energy produced in regions of large velocity gradients. This was first noted by Taylor [20] and later, Burgers [4] found an exact solution to the Navier-Stokes equations for a constant density fluid that modeled these processes. Burgers' solution may be obtained by first decomposing the velocity field in Cartesian coordinates (x, y, z) into an irrotational part corresponding to pure strain $\mathbf{u}_s = (\alpha x, \beta y, \gamma z)$ with $\alpha+\beta+\gamma = 0$, and a rotational part confined to the x-y plane, $\mathbf{u}_\omega = (u, v, 0)$. The only nonzero component of the vorticity, $\vec{\omega} = \nabla \times \mathbf{u}$ is that in the z-direction, $\vec{\omega} = (0, 0, \omega)$, and the relevant vorticity equation then reduces to

$$\frac{\partial \omega}{\partial t} + (\alpha x + u)\frac{\partial \omega}{\partial x} + (\beta y + v)\frac{\partial \omega}{\partial y} = \gamma\omega + \nu\nabla^2\omega, \tag{1.1}$$

$$\nabla^2\psi = -\omega, \quad u = \frac{\partial \psi}{\partial y}, \quad v = -\frac{\partial \psi}{\partial x}. \tag{1.2}$$

For the case of axisymmetric strain, $\alpha = \beta = -\gamma/2$, $\gamma > 0$, a steady solution of (1-2) is

$$\omega = \frac{\gamma\Gamma}{4\pi\nu} e^{-\gamma(x^2+y^2)/4\nu} \tag{1.3}$$

which induces the angular velocity,

$$\hat{u_{\theta 0}} = \frac{\Gamma}{2\pi r}\left(1 - e^{-\frac{\gamma r^2}{4\nu}}\right), \tag{1.4}$$

where Γ is the total circulation. We will refer to this solution as the axisymmetric Burgers vortex with the Reynolds number defined as $R = \Gamma/2\pi\nu$. For the case of

plane strain $\alpha = \gamma$, $\beta = 0$, $\gamma > 0$, a steady flow solution of (1.1)-(1.2) is

$$\omega = \omega_0 e^{-\gamma x^2/2\nu} \tag{1.5}$$

where ω_0 is the maximum vorticity. This solution is often referred to as the Burgers vortex layer.

1.1.1 Relevance to turbulence

Burgers vortices have been used to model various features of turbulence including the energy spectrum in the range of dissipation wavenumbers (Townsend [21]) and the nearly-streamwise vortices which form in the braid region of the temporal mixing layer (Lin and Corcos [13]). Interest in the properties of the Burgers vortex intensified following large scale numerical simulations of turbulence, for example Kerr[10], Vincent and Meneguzzi [22], She *et al.* [19], Ashurst *et al.* [2], Reutsch and Maxey [16] and others, which indicated that regions of high vorticity seemed to "self-organize" into tube-like structures. Ashurst *et al.* [2] demonstrated a moderate correlation between the direction of the vorticity vector and that of the strain eigenvector corresponding to the intermediate eigenvalue and this, together with the tube observation, revived interest in the Townsend-Burgers model of the fine scales. Whilst the structure of the Burgers vortex may be too simple to explain the principal characteristics of the probability distribution of the longitudinal velocity gradients (Saffman and Pullin [15]), the numerical experiments of Jiménez *et al.* [9], do provide evidence that the structure of the most intense vorticity, which occupies a small fraction of the fluid volume and provides a small fraction of the dissipation, but which may yet may be responsible for the tails of the velocity-gradient probability density functions, closely resembles Burgers vortices. Furthermore, Jiménez and Wray [8] note that whenever vortices are strongly stretched, the radius approaches the Burgers limit, and that the cross section of these long coherent vortices will be elliptical in nature.

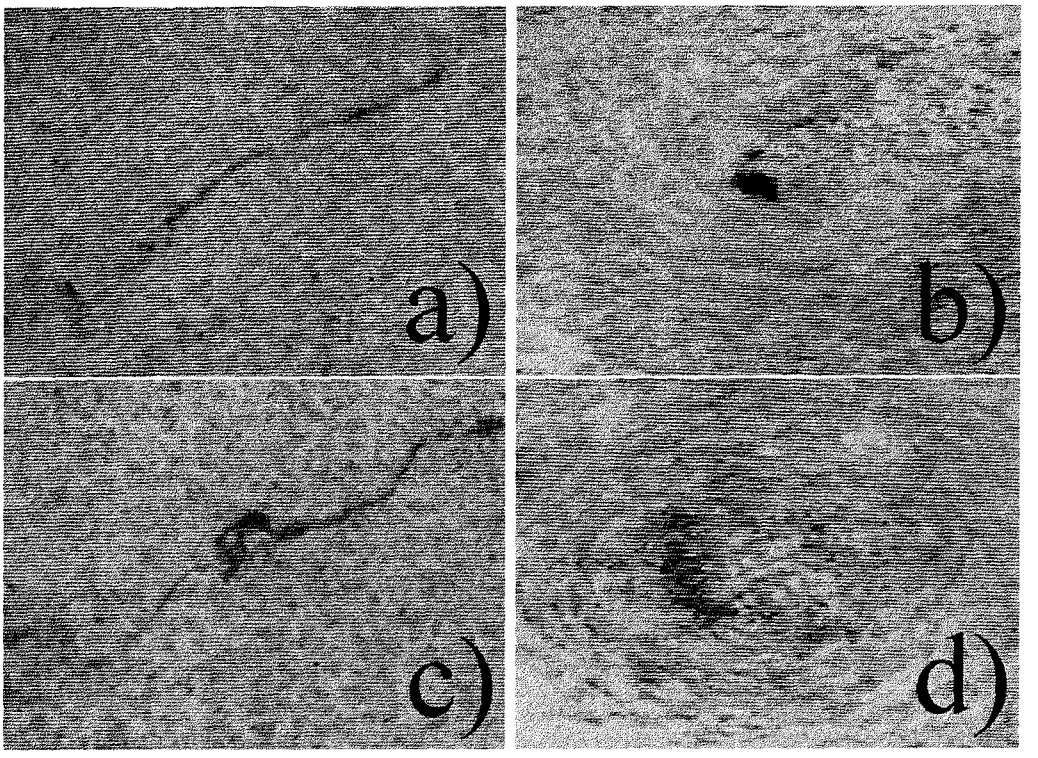

Figure 1.1: Flow visualization by Douady, *et al.*[5] showing intensification of vorticity in to long, thin, tube-like structures. The Reynolds number is $80,000$. Subfigures a)–b) show axial and side views of the initial formation of a tube of length $\sim 5cm$ and diameter $\sim 0.1mm$. Subfigures c)–d) show the views of the tube $0.1s$ later.

1.1.2 Stability

Leibovich and Holmes [12] addressed the global stability of the axisymmetric Burgers vortex using an energy method but found that there existed no finite critical viscosity at which the vortex became unstable. They noted that this did not indicate stability to all perturbations. Robinson and Saffman [17], henceforth referred to as RS84, using perturbation methods, solved the corresponding linearized stability problem through a series expansion in R, finding the Burgers vortex to be linearly stable for small R. Buntine and Pullin [3] studied the merger and cancellation of Burgers vortices in order to model the dissipation range energy spectrum for three-dimensional isotropic turbulence.

1.2 Stretched vortices in nonsymmetric strain

1.2.1 Symmetry considerations

Direct numerical simulations not only suggest the existence of vortex structures, but also the tendency of these structures to persist over long periods of time, even when their length reaches the integral scale of the flow (Vincent [22]). Flow visualization by Douady *et al.* [5] (see Figure 1.1) of homogeneous turbulence has also shown the persistence of intense vortex tubes. In all these cases it seems reasonable to suppose that the vortex tubes were present in regions where the strain was not perfectly axially symmetric, suggesting the relevance of nonsymmetric Burgers vortices. Here it is convenient to consider, without loss of generality, cases where $\alpha < 0 \leq \gamma$, $\beta \geq \alpha$ and define the field in terms of a single parameter, the strain ratio, λ, where

$$\begin{aligned} \alpha &= -\tfrac{1}{2}(1+\lambda)\gamma, \\ \beta &= -\tfrac{1}{2}(1-\lambda)\gamma, \\ \lambda &= \tfrac{\alpha-\beta}{\alpha+\beta}. \end{aligned} \tag{1.6}$$

The strain ratio is non-negative and uniquely defines the strain into the following classifications:

$\lambda = 0,$	$\alpha = \beta = -\gamma/2,$	axisymmetric axial strain
$0 < \lambda < 1,$	$\alpha < \beta < 0,$	nonsymmetric axial strain
$\lambda = 1,$	$\alpha = -\gamma, \beta = 0,$	plane strain
$1 < \lambda < 3,$	$\beta > 0, \beta < \gamma,$	biaxial strain
$\lambda = 3,$	$\alpha = -2\gamma, \beta = \gamma,$	axisymmetric biaxial strain
$\lambda > 3,$	$\beta > \gamma,$	extreme biaxial strain

where, for $\lambda > 3$, it should be noted that the z-direction is no longer the direction of maximum extensional strain.

1.2.2 Vortex structure

RS84 first proposed the generalized or *nonsymmetric* Burgers vortex corresponding to strain geometries intermediate between axisymmetric and plane strain. They numerically found steady solutions at Reynolds numbers up to 100 and strain ratios $0.25 \leq \lambda \leq 0.75$. They showed that increased nonsymmetry of the strain tended to increase the ellipticity of the vortex while increasing the circulation decreased the ellipticity and rotated the vortex counterclockwise to a limit where the vortex was aligned 45° to the axes of the strain. Kida and Ohkitani [11], in a study of the spatiotemporal intermittency of a developed turbulence, found that vorticity tended to be concentrated in long thin tubelike regions that resemble nonsymmetric Burgers Vortex in structure. Moffatt, Kida, and Ohkitani [14], which we will refer to as MKO94, developed a large Reynolds number asymptotic theory of stretched vortices in nonsymmetric straining fields. The structure of the vortices for the small parameter, λ/R, was given as a correction to that of a Burgers vortex. Jiménez, *et al.* [7] showed the asymptotic results from MKO94 to be valid in a larger, elliptical region. Furthermore, they provide evidence of vortices with elliptical structure in a numerical simulation of decaying two-dimensional turbulence.

1.2.3 Stability

No comprehensive analysis of the stability of nonsymmetric Burgers vortices has been presented thus far. Buntine and Pullin [3] calculated several examples of the relaxation of an initial vorticity distribution towards a nonsymmetric state, indicating at least some measure of the stability to two-dimensional disturbances for $\lambda < 1$. MKO94 argued that the stretched vortices can survive for long times even when two of the principal rates of strain become positive. From a far field analysis of the vorticity, they indicate that for biaxial strain, vorticity away from the core of the vortex will behave like a passive scalar and be convected to infinity, therefore eliminating the possibility of a true steady solution in the region $\lambda > 1$.

1.3 Outline

The layout of this thesis is as follows. We begin in Chapter 2 by by utilizing an extension of the pseudo-spectral method of RS84 to calculate solutions of the Navier-Stokes equations corresponding to steady nonsymmetric Burgers vortices, over a wide range of (R-λ) space. When R is large and $\lambda > 1$ we have no difficulty in obtaining apparently steady solutions with vorticity at the level of machine precision far from the vortex core. When $\lambda \gg 1$, our numerical results suggest a method for obtaining an approximate analytical form for the vorticity field outside the region studied by MKO94 but confined by the strain to a cat's-eye shaped region of nearly two-dimensional flow. This approximation, developed in Chapter 3, confirms the exponentially small vorticity away from the core and also provides a means of estimating the exponentially slow leakage and convection to infinity of vorticity from the confinement zone. Our estimate of the decay rate of the circulation differs substantially from MKO94.

A full numerical normal-mode treatment of the stability of the axisymmetric Burgers vortex is given in Chapter 4. It is found that the axisymmetric vortex is stable to two-dimensional disturbances, in which velocity perturbations are restricted to the plane normal to the vorticity, for all Reynolds numbers. A Lagrangian convectively neutral mode corresponding to an arbitrary bulk displacement of a compact vorticity distribution embedded in a general linear velocity field is identified. When applied to the steady generalized Burgers vortex, this implies a convectively neutral stability which convects the vortex to infinity without change of form when $\lambda > 1$. The normal mode stability of the numerically obtained nonsymmetric steady vortex solutions is studied in Chapter 5 using an extension of the power method. For the cases studied at $R = 1$, 10, 100 and 1000, when $0 < \lambda < 1$ (nonsymmetric axial strain), the largest eigenvalue always corresponds to the above-mentioned convectively neutral instability mode which, for this range of λ, convects small bulk displacement of the vorticity field into the undisturbed center of vorticity. This implies stability of the nonsymmetric Burgers vortices for $0 \leq \lambda < 1$, for all R. When $\lambda > 1$, the convectively neutral mode is also found and the algebraically second largest eigenvalue is

zero to the accuracy of our calculation. In an appendix, the steady exact solution to the Navier-Stokes corresponding to the Sullivan vortex is shown to be stable to two dimensional disturbances.

Chapter 2 Structure of Nonsymmetric Burgers Vortices

2.1 Basic equations

Unless otherwise noted, all quantities are henceforth nondimensionalized using the length and time scales $\sqrt{2\nu/\gamma}$ and $2/\gamma$ respectively. Equations (1.1)-(1.2) become

$$\frac{\partial\omega}{\partial t} = \frac{\partial^2\omega}{\partial x^2} + \frac{\partial^2\omega}{\partial y^2} + [(1+\lambda)x - Ru]\frac{\partial\omega}{\partial x} + [(1-\lambda)y - Rv]\frac{\partial\omega}{\partial y} + 2\omega, \tag{2.1}$$

$$\nabla^2\psi = -\omega, \quad u = \frac{\partial\psi}{\partial y}, \quad v = -\frac{\partial\psi}{\partial x}, \tag{2.2}$$

where ω, u, v, x, y, and t, now denote dimensionless variables without change of notation. This equation has three notable solutions. First, there is the axisymmetric Burgers vortex solution, valid for all R at $\lambda = 0$,

$$\omega = Re^{-(x^2+y^2)/2}. \tag{2.3}$$

Second, we have,

$$\omega = \sqrt{1-\lambda^2}\; e^{-\frac{1}{2}\left((1+\lambda)x^2+(1-\lambda)y^2\right)}, \tag{2.4}$$

which is valid for all λ at $R = 0$, and third, for plane strain, there exists the Burgers vortex-layer solution,

$$\omega = \omega_0 e^{-x^2}, \tag{2.5}$$

which holds for $\lambda = 1$ for all ω_0, but does not correspond to a confined vorticity distribution and will not be studied presently, but is referred to in Chapter 3.

2.2 Numerical method

2.2.1 Pseudo-spectral method

Here we investigate numerically steady solutions to (2.1) for general $\lambda > 0$. We assume that $\omega(x,y)$ decays exponentially when $r = (x^2+y^2)^{1/2} \to \infty$ independent of direction. This allows use of a collocation method to approximate the vorticity with the double series of sinc functions in x and y (see RS84),

$$\omega(x,y) = \sum_{k=-M}^{M} \sum_{l=-N}^{N} \omega_{kl} S(k,h_x;x) S(l,h_y;y), \tag{2.6}$$

where

$$S(j,h;\zeta) = \frac{\sin[(\pi/h)(\zeta - jh)]}{(\pi/h)(\zeta - jh)} \tag{2.7}$$

in a rectangular domain defined by $-h_x M ... h_x M \times -h_y N ... h_y N$ where ω_{kl} are coefficients to be determined and M, N are specified series-truncation parameters. Integration and differentiation of the sinc function can be approximated using

$$\begin{aligned} \int_{-\infty}^{+\infty} \omega(x,y)dx &= h_x \sum_{k=-M}^{M} \sum_{l=-N}^{N} \omega_{kl} S(l,h_y;y) \\ \frac{\partial^n \omega}{\partial x^n}(x,y) &= \sum_{k=-M}^{M} \sum_{l=-N}^{N} \left(h_x^{-n} \sum_{p=-M}^{M} \delta_{pk}^{(n)} \omega_{pl} \right) S(k,h_x;x) S(l,h_y;y). \end{aligned} \tag{2.8}$$

We will only need $n = 1, 2$, for which

$$\delta_{mn}^{(1)} = \frac{(-1)^{n-m}}{n-m}(1-\delta_{nm}), \quad \delta_{nm}^{(2)} = -\frac{\pi^2}{3}\delta_{nm} - \frac{2(-1)^{n-m}}{(n-m)^2}(1-\delta_{nm}). \tag{2.9}$$

On substituting (2.6) into (1.2), the Poisson equation may be solved in terms of the Fourier transform of the vorticity, $\widehat{\omega}$, to give the approximated velocities at each of the collocation points as

$$\widehat{\omega}(\xi,\eta) = h_x h_y e^{i(\xi k h_x + \eta l h_y)} \left[H(\xi + \frac{\pi}{h_x}) - H(\xi - \frac{\pi}{h_x}) \right] \left[H(\eta + \frac{\pi}{h_y}) - H(\eta - \frac{\pi}{h_y}) \right] \tag{2.10}$$

where H is the heaviside function. This yields approximated velocities at each of the collocation points as

$$u = -\frac{\partial \psi}{\partial y} = \frac{-i}{(2\pi)^2} \int\int \frac{\eta \hat{\omega}}{\xi^2 + \eta^2} e^{-i(\xi x + \eta y)} d\xi d\eta, \tag{2.11}$$

$$v = \frac{\partial \psi}{\partial x} = \frac{i}{(2\pi)^2} \int\int \frac{\xi \hat{\omega}}{\xi^2 + \eta^2} e^{-i(\xi x + \eta y)} d\xi d\eta. \tag{2.12}$$

From this, the coefficients of the expansion of the velocities in terms of sinc functions are

$$u_{i,j} = -\frac{h_x}{\pi} I^{(1)}_{j-l,i-k}, \qquad v_{i,j} = \frac{h_y}{\pi} I^{(2)}_{i-k,j-l}, \tag{2.13}$$

where

$$I^{(1)}_{m,n} = \int_0^1 \int_0^1 \frac{\alpha \eta}{\alpha^2 \xi^2 + \eta^2} \sin((j-l)\pi\eta) \cos((i-k)\pi\xi) d\xi d\eta, \tag{2.14}$$

$$I^{(2)}_{m,n} = \int_0^1 \int_0^1 \frac{\alpha \xi}{\alpha^2 \xi^2 + \eta^2} \sin((i-k)\pi\xi) \cos((j-l)\pi\eta) d\xi d\eta. \tag{2.15}$$

Due to the difficulty evaluating these double integrals, it is more efficient to calculate $I_{m,n}$ numerically using,

$$\begin{aligned} I^{(1)}_{m,n} &= \int_0^1 \frac{\alpha}{1+\alpha^2 x^2} \left[\frac{\sin^2[(m\pi + n\pi x)/2]}{m\pi + n\pi x} + \frac{\sin^2[(m\pi - n\pi x)/2]}{m\pi - n\pi x} \right] dx, \\ &+ \int_0^1 \frac{\alpha}{\alpha^2 + x^2} \left[\frac{\sin^2[(m\pi x + n\pi)/2]}{m\pi x + n\pi} + \frac{\sin^2[(m\pi x - n\pi)/2]}{m\pi x - n\pi} \right] dx, \end{aligned} \tag{2.16}$$

$$\begin{aligned} I^{(2)}_{m,n} &= \int_0^1 \frac{\alpha}{\alpha^2 + x^2} \left[\frac{\sin^2[(m\pi + n\pi x)/2]}{m\pi + n\pi x} + \frac{\sin^2[(m\pi - n\pi x)/2]}{m\pi - n\pi x} \right] dx, \\ &+ \int_0^1 \frac{\alpha}{1+\alpha^2 x^2} \left[\frac{\sin^2[(m\pi x + n\pi)/2]}{m\pi x + n\pi} + \frac{\sin^2[(m\pi x - n\pi)/2]}{m\pi x - n\pi} \right] dx. \end{aligned} \tag{2.17}$$

Then, by inserting (2.6) into (2.1) and using (2.8), we obtain

$$\begin{aligned} F_{ij} &= \frac{1}{h_x^2} \sum_{k=-M}^{M} \delta^{(2)}_{ki} \omega_{kj} + \frac{1}{h_y^2} \sum_{l=-N}^{N} \delta^{(2)}_{lj} \omega_{il} + 2\omega_{ij} \\ &+ [(1+\epsilon)i - \frac{R}{h_x} u_{ij}] \sum_{k=-M}^{M} \delta^{(1)}_{ki} \omega_{kj} + [(1-\epsilon)j - \frac{R}{h_y} u_{ij}] \sum_{l=-N}^{N} \delta^{(1)}_{lj} \omega_{il}, \end{aligned} \tag{2.18}$$

where

$$u_{i,j} = -\frac{h_x}{\pi} \sum_{k=-M}^{M} \sum_{l=-N}^{N} I^{(1)}_{j-l,i-k} \omega_{kl}, \qquad v_{i,j} = \frac{h_y}{\pi} \sum_{k=-M}^{M} \sum_{l=-N}^{N} I^{(2)}_{i-k,j-l} \omega_{kl}. \tag{2.19}$$

Two constraints to this equation are applied; first, we fix the total circulation and second, we fix the centroid of vorticity in accordance with RS84. The circulation is fixed at 2π by adding the term $\rho(i,j)\left(h_x h_y \sum_{k=-M}^{M} \sum_{l=-N}^{N} \omega_{kl} - 2\pi\right)$ to (2.18) where $\rho(i,j)$ is a random number function that decouples the last term from the other equations. Second, since the equations are invariant under a 180° rotation, $F_{ij} = F_{-i,-j}$, we can fix the centroid of vorticity at the origin and also reduce the number of unknowns to $(2M+1)N + M + 1$.

2.2.2 Accuracy

With M and N fixed, this system is solved using Newton-Raphson method where the Jacobian is $J_{ijkl} = \partial F_{ij}/\partial x_{kl}$. Euler continuation in λ starting from the axisymmetric Burgers vortex is used to expedite results, but this is not necessary for convergence, which is defined by $|J_{ijkl}(\omega^{new}_{kl} - \omega^{old}_{kl})|_{\max} < 10^{-12}$ and $|\omega_{\text{boundary}}/R|_{\max} < 10^{-5}$. Second order convergence is always obtained within a few iterations. Given that the Jacobian contains $((2M+1)N + M + 1)^2$ elements, we were limited by storage capacity to a maximum square domain of $M, N = 50$, rather than by a CPU time constraint.

In order to determine the best possible values for the basis spacing h_x and h_y, the code is tested using the axisymmetric case and it is found, by trial and error, that both the error from the Newton-Raphson method and the maximum value of the vorticity at the boundary are minimized by using $h_x = \sqrt{\pi/M}$ and $h_y = \sqrt{\pi/N}$, leading to a domain size of $\sqrt{\pi M} \times \sqrt{\pi N}$. Since the Burgers vortex is axisymmetric, the best domain shape corresponds to a square, $M = N$, but choice of domain aspect ratio depends quite strongly on the shape of the function to be approximated. At low Reynolds numbers, strain tends to elongate the vortex, therefore a rectangular domain can be used for greater accuracy. At higher Reynolds numbers, the vortex tends to be less elliptical, thus $M = N$ is used as before, but since the vortex aligns

itself at an angle to the strain, domain size efficiency can be maximized by allowing strain to be rotated through an angle, ϕ, where the velocities are

$$u_x = \alpha x \cos^2\phi + \beta x \sin^2\phi + \frac{\beta-\alpha}{2} y \sin 2\phi, \tag{2.20}$$

$$u_y = \beta y \cos^2\phi + \alpha y \sin^2\phi + \frac{\beta-\alpha}{2} x \sin 2\phi, \tag{2.21}$$

choosing ϕ to align the major axis of the vortex with diagonal of the domain.

2.3 Results

Since exact solutions (2.3)–(2.4) are known for either $R = 0$ or $\lambda = 0$, the R-λ parameter space for Reynolds numbers $1 < R < 10^4$ and $0.2 < \lambda < 150$ is investigated. For each case studied, Tables 2.1–2.5 show the value of the core vorticity and the largest value of the vorticity at the domain boundary. Ideally, this latter quantity should be at the level of machine precision. In Figures 2.7–2.30, the isovorticity contours and the streamlines projected onto the plane normal to ω are plotted on the domain on which they are calculated. The isovorticity contour plots show the directions of the principal axes of strain and contours varying from $0.1R$ to the lowest value, given separately on each plot. The projected streamlines correspond to globally inward flow when $\lambda \leq 1$ but for $\lambda > 1$ some of the contours shown correspond to fluid particles that are not being swept into the vortex. Our results can be classified into three categories, denoted by low, intermediate, or high Reynolds numbers.

In the low Reynolds number region, $R = 1$–10 (Tables 2.1–2.2, Figures 2.1–2.11) the axes of strain are rotated by 45° to achieve maximum accuracy. All plots are shown on the domain of calculation and the principal axes of strain are shown at the origin of each isovorticity plot. The vorticity contours are stretched in the y-direction and due to this, steady solutions cannot be accurately calculated within our bounded domain beyond $\lambda > 0.8$. This behavior can be predicted by assuming that low Reynolds number flow can be approximated by the zero Reynolds number limit (2.4) and it is likely that this is why RS84 stated that as $\lambda \to 1$ the "elongation of the

vortex tends to infinity" and only investigated solutions for $\lambda \leq 0.75$. The streamlines are shown for completeness and for comparison to higher Reynolds number cases.

Table 2.1: Vorticity values at the core and the boundary $R = 1$ with $M, N = 40$, $\phi = \pi/4$.

λ	ω_{core}/R	$\omega_{\max}\|_{\text{boundary}}/R$
0.2	0.9802	2.23E-16
0.4	0.9179	9.27E-16
0.6	0.8025	8.66E-16
0.8	0.6027	1.00E-10

Table 2.2: Vorticity values at the core and the boundary for $R = 10$ with $M, N = 40$, $\phi = \pi/4$.

λ	ω_{core}/R	$\omega_{\max}\|_{\text{boundary}}/R$
0.2	0.9932	6.62E-13
0.4	0.9711	2.35E-11
0.6	0.9268	1.15E-10
0.8	0.8332	1.77E-10

For intermediate values of the Reynolds number, $R = 100$ (Table 2.3, Figures 2.13–2.18), it is clear that elongation of the vortex does not tend to infinity as $\lambda \to 1$. In fact, increasing the circulation tends to reduce the ellipticity of the vortex as well as rotating the major and minor axes of the vortex at an angle that approaches 45° for large R (originally noted in RS84). This enables a steady solution to be found for $\lambda = 1$, as shown in Figure 2.15, which, in contrast to the vortex sheet (1.5), is a bounded vorticity solution in plane strain. Furthermore, at this Reynolds number, we are easily able to find numerically steady solutions for $\lambda > 1$. The solution for $\lambda = 1.5$ is shown in Figure 2.17, but extra care must be given to solutions in this region. As shown in Figure 2.18, for $\lambda > 1$, stagnation points will appear in the flow. MKO94 argued that the vorticity beyond the stagnation points will be transcendentally small and therefore be convected away from the vortex as a passive scalar. However, their estimate for vorticity flux due to this phenomena is exceedingly small and this time

variation does not seem to compromise our ability to find numerically steady solutions for $\lambda > 1$. Instead, our solutions correspond to a "snapshot" of the vorticity at a time when the majority of the vorticity is contained within our bounded domain. To account for this, we will call our steady solutions "quasi-steady" and later, in Chapter 3, address the time variation and the nature of the vorticity flux.

Table 2.3: Vorticity values at the core and the boundary for $R = 100$.

λ	M	N	ϕ	ω_{core}/R	$\omega_{\max}\|_{\text{boundary}}/R$
0.5	40	40	0	0.9993	1.79E-12
1.0	50	50	0	0.9974	6.19E-15
1.5	40	40	$\pi/3$	0.9939	1.08E-8
2.0	50	50	$-\pi/6$	0.9888	4.95E-6
2.5	20	80	0	0.9811	9.13E-5

For very large Reynolds numbers, $R = 10^3$–10^4 (Tables 2.4-2.5, Figures 2.19–2.30), variation away from the the Burgers solution (2.3) is very small except for large strain ratios, well into the biaxial region. In this region, we notice that the vorticity contours closely relate to the projected streamlines (compare Figures 2.25–2.30). Since the vorticity is exponentially small outside of the core, it is being passively convected by the velocity field. The projected streamlines closely resemble the streamlines for a point vortex in pure two-dimensional strain, except that since the vortex is being stretched, there is some inward flow which causes the streamlines to slowly coil into the origin.

Table 2.4: Vorticity values at the core and the boundary $R = 1000$ with $M, N = 50$, $\phi = 0$.

λ	ω_{core}/R	$\omega_{\max}\|_{\text{boundary}}/R$
1.0	0.99997	1.96E-14
2.0	0.99989	2.01E-14
3.0	0.99976	2.44E-14
6.0	0.99905	1.26E-14

Table 2.5: Vorticity values at the core and the boundary $R = 10,000$ with $M, N = 50$, $\phi = 0$.

λ	ω_{core}/R	$\omega_{\text{max}}\|_{\text{boundary}}/R$
50.0	0.99934	2.44E-14
100.0	0.99734	1.89E-8
150.0	0.9940	1.26E-6

The viscous energy dissipation, which is given by $\Phi = 2\nu s_{ij} s_{ij}$, where

$$[s_{ij}] = \begin{bmatrix} \alpha + \frac{\partial u_x}{\partial x} & \frac{1}{2}\left(\frac{\partial u_x}{\partial y} + \frac{\partial u_y}{\partial x}\right) & 0 \\ \frac{1}{2}\left(\frac{\partial u_x}{\partial y} + \frac{\partial u_y}{\partial x}\right) & \beta + \frac{\partial u_y}{\partial y} & 0 \\ 0 & 0 & \gamma \end{bmatrix}, \tag{2.22}$$

is plotted for $R = 10$–$1,000$ in Figures 2.32–2.34. In the case of the axisymmetric Burgers vortex, the maximum dissipation occurs in a ring at the boundary of the core of the vortex. For low Reynolds numbers the nonsymmetric strain deforms this region of maximum dissipation into two distinct lobes. For intermediate and high Reynolds numbers, a crescent shape area of the maximum dissipation is found. At high Reynolds numbers the dissipation contours are nearly identical for the cases of $\lambda = 1.0, 3.0, 6.0$ It is interesting to note the agreement between energy dissipation shown in Figures 2.32–2.34 and Fig. 7 from MKO94 calculated based on their asymptotic expansion in $1/R_\Gamma$, even for for the fairly low Reynolds number case, $R = 10$.

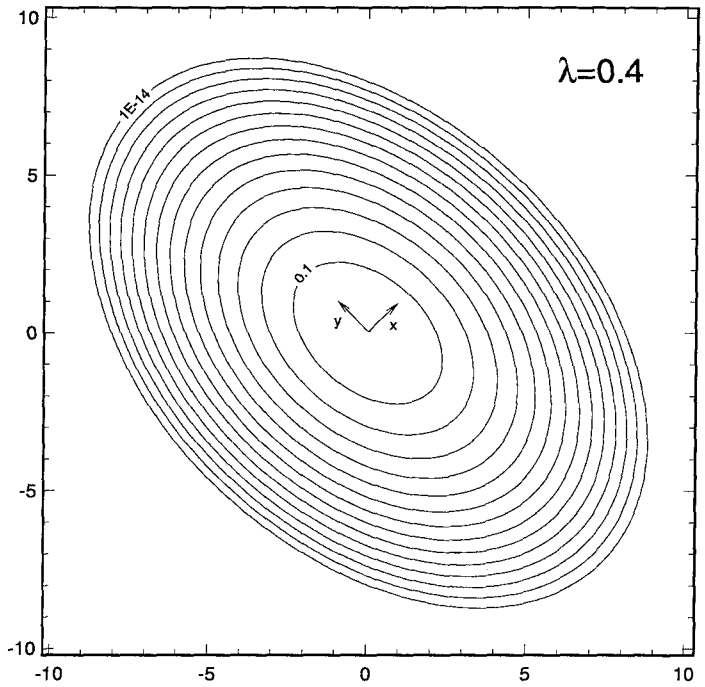

Figure 2.1: Isovorticity contours for $R = 1$, $\lambda = 0.4$, $M, N = 40$. Note the direction of principal axes of strain shown at the origin.

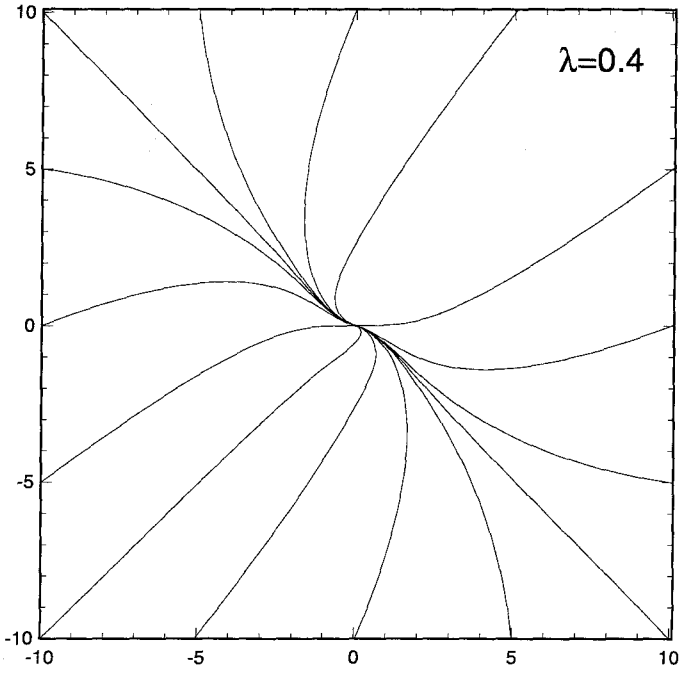

Figure 2.2: Projected Streamlines for $R = 1$, $\lambda = 0.4$, $M, N = 40$.

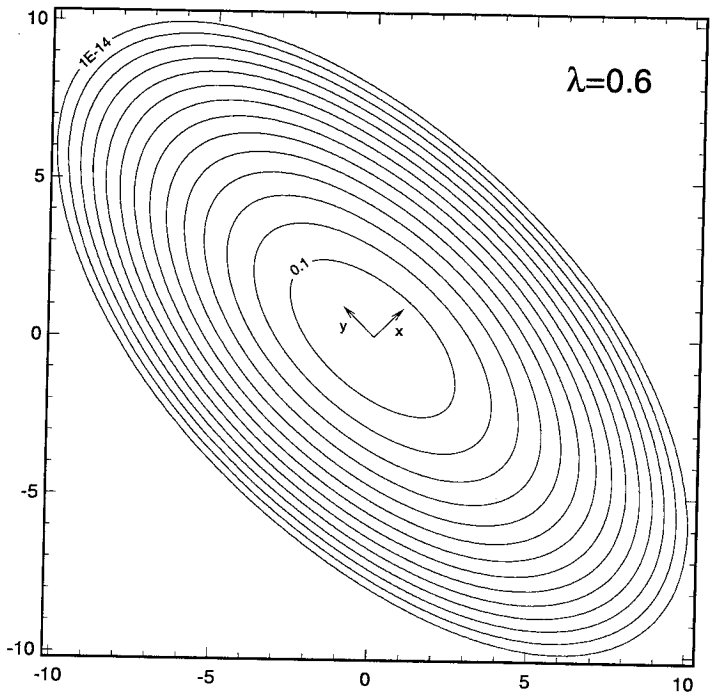

Figure 2.3: Isovorticity contours for $R = 1$, $\lambda = 0.6$, $M, N = 40$. Note the direction of principal axes of strain shown at the origin.

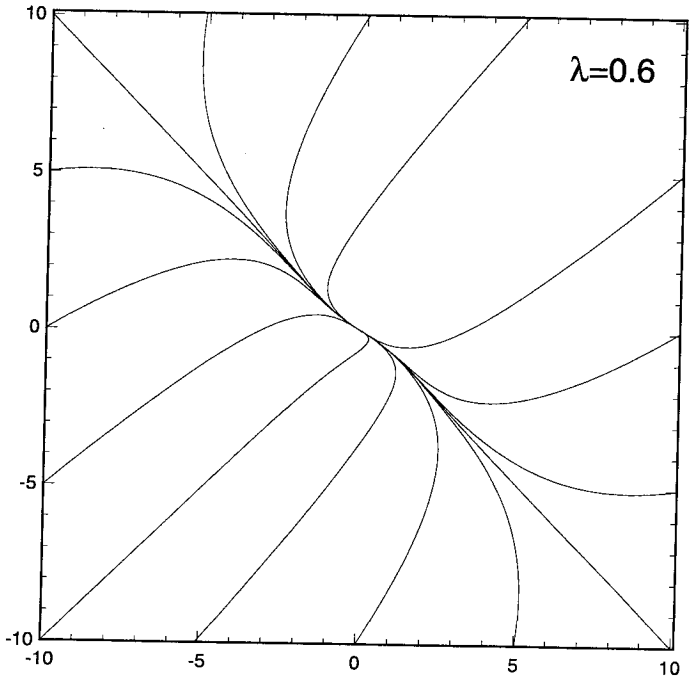

Figure 2.4: Projected Streamlines for $R = 1$, $\lambda = 0.6$, $M, N = 40$.

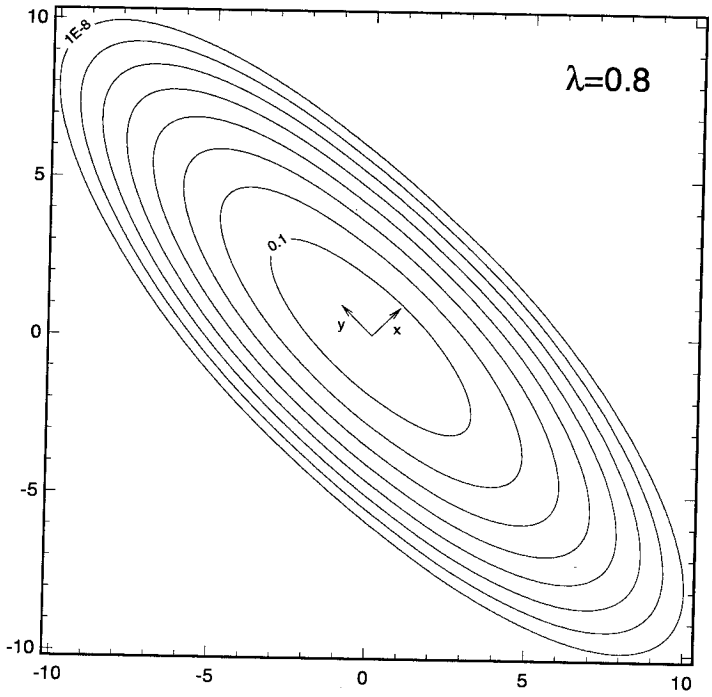

Figure 2.5: Isovorticity contours for $R = 1$, $\lambda = 0.8$, $M, N = 40$. Note the direction of principal axes of strain shown at the origin.

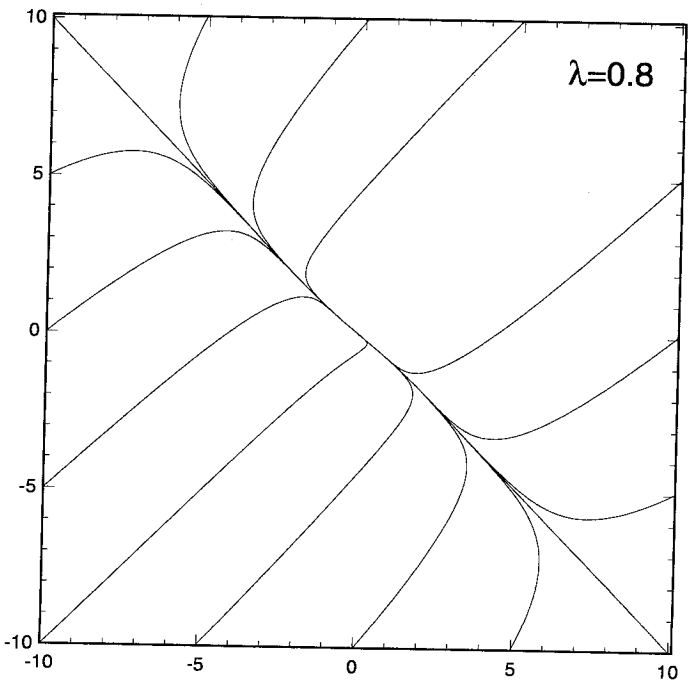

Figure 2.6: Projected Streamlines for $R = 1$, $\lambda = 0.8$, $M, N = 40$.

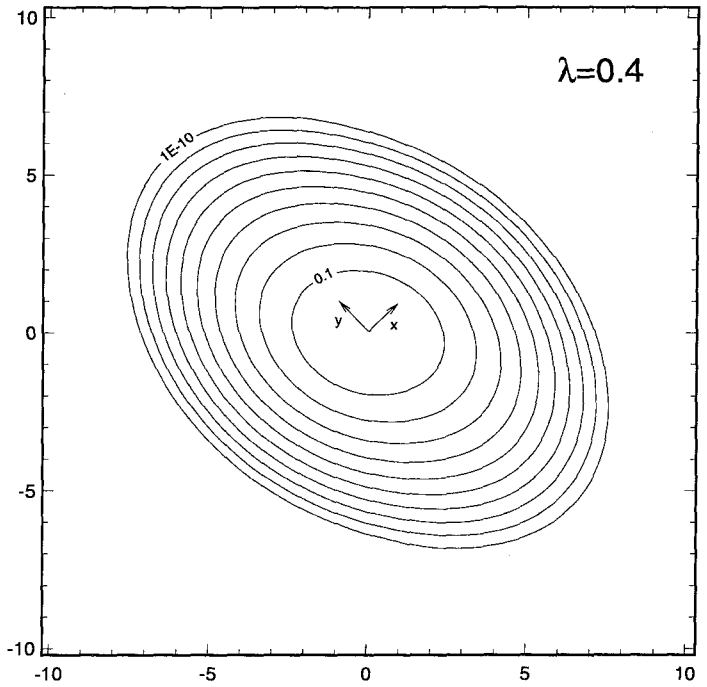

Figure 2.7: Isovorticity contours for $R = 10$, $\lambda = 0.4$, $M, N = 40$. Note the direction of principal axes of strain shown at the origin.

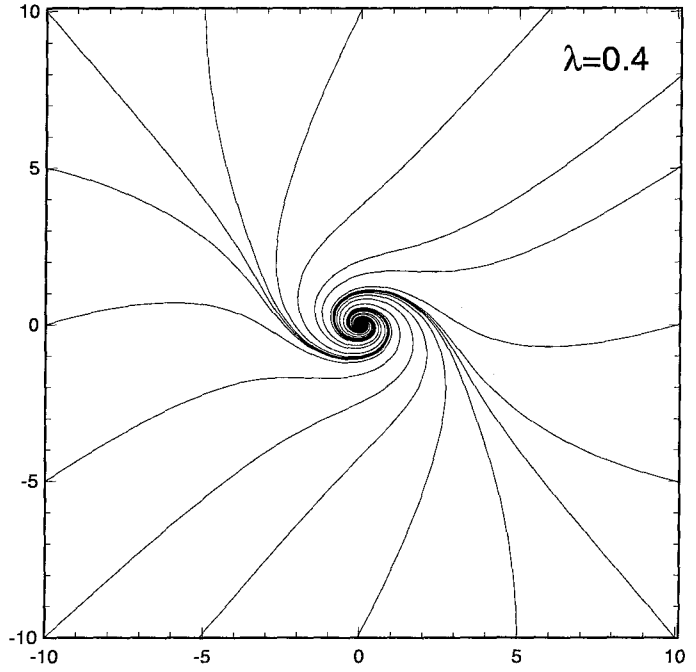

Figure 2.8: Projected Streamlines for $R = 10$, $\lambda = 0.4$, $M, N = 40$.

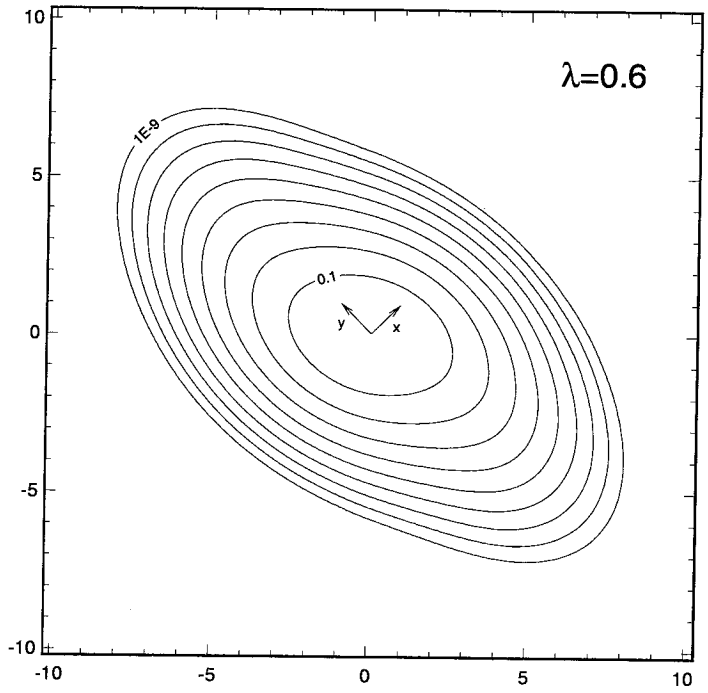

Figure 2.9: Isovorticity contours for $R = 10$, $\lambda = 0.6$, $M, N = 40$. Note the direction of principal axes of strain shown at the origin.

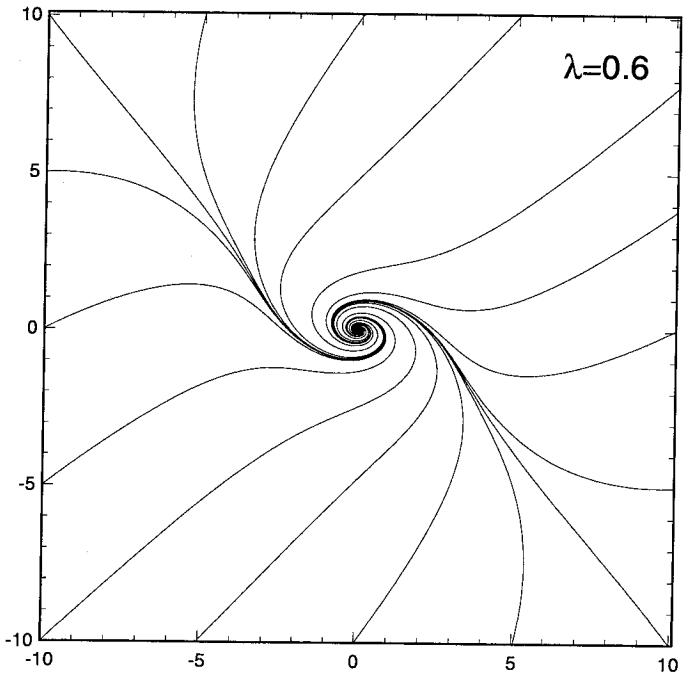

Figure 2.10: Projected Streamlines for $R = 10$, $\lambda = 0.6$, $M, N = 40$.

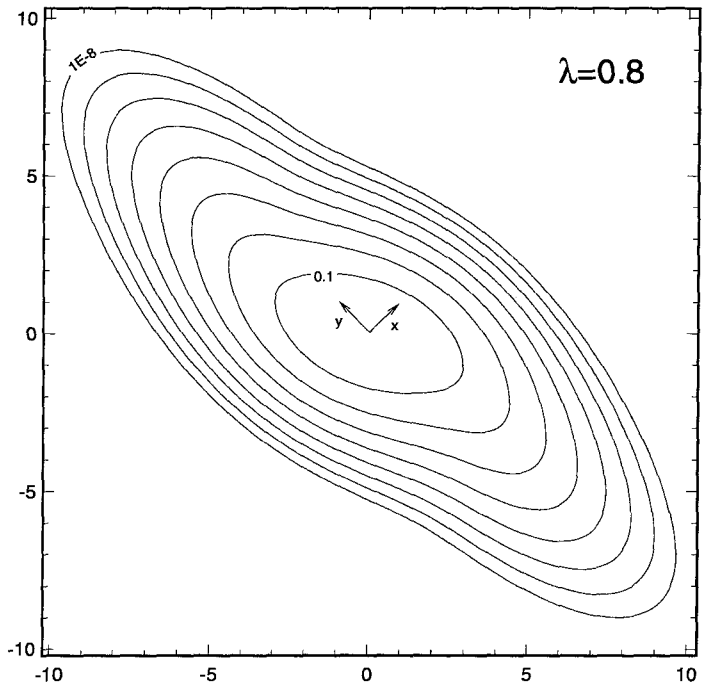

Figure 2.11: Isovorticity contours for $R = 10$, $\lambda = 0.8$, $M, N = 40$. Note the direction of principal axes of strain shown at the origin.

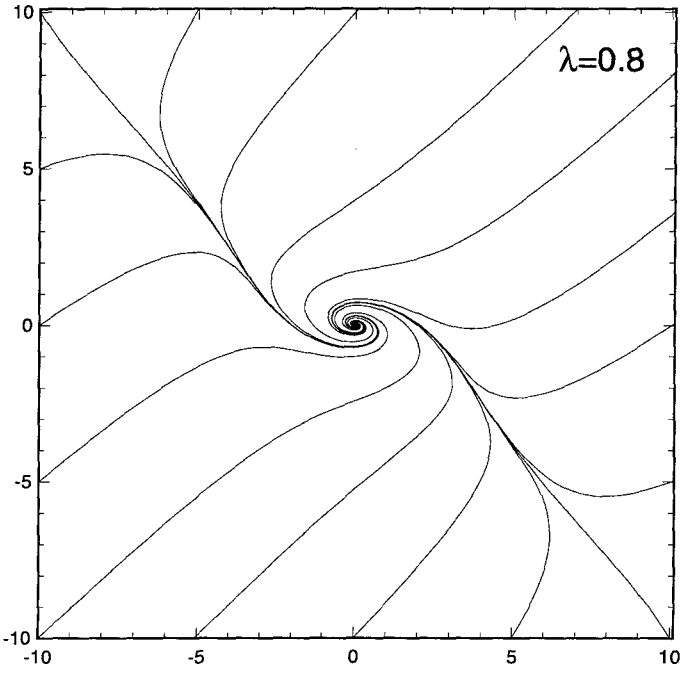

Figure 2.12: Projected Streamlines for $R = 10$, $\lambda = 0.8$, $M, N = 40$.

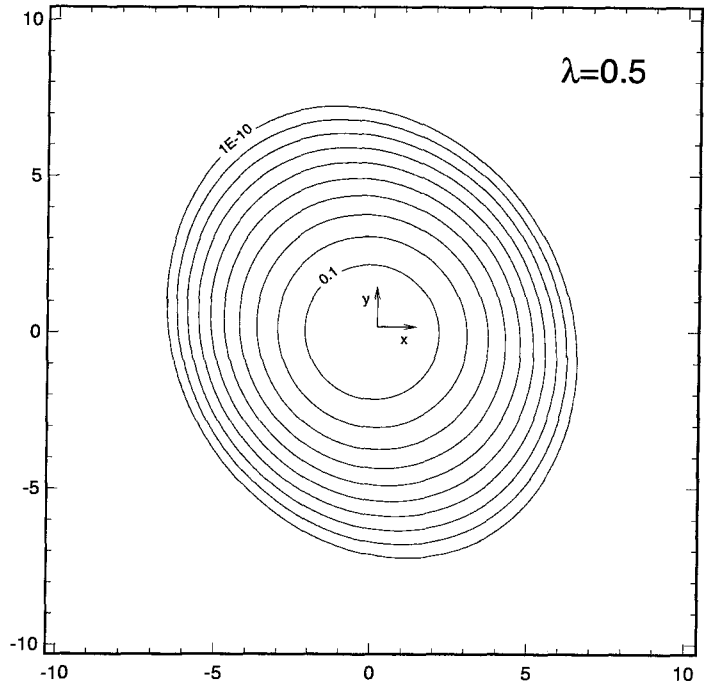

Figure 2.13: Isovorticity contours for $R = 100$, $\lambda = 0.5$, $M, N = 40$.

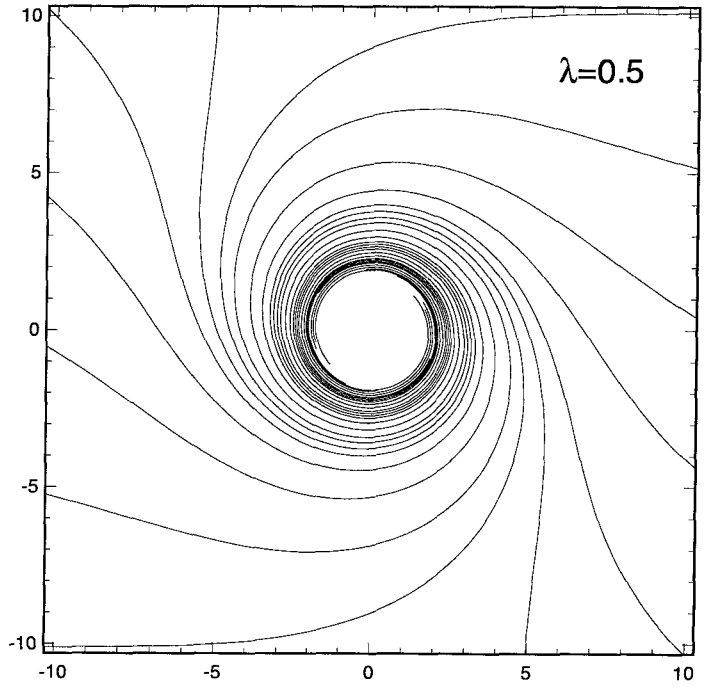

Figure 2.14: Projected Streamlines for $R = 100$, $\lambda = 0.5$, $M, N = 40$.

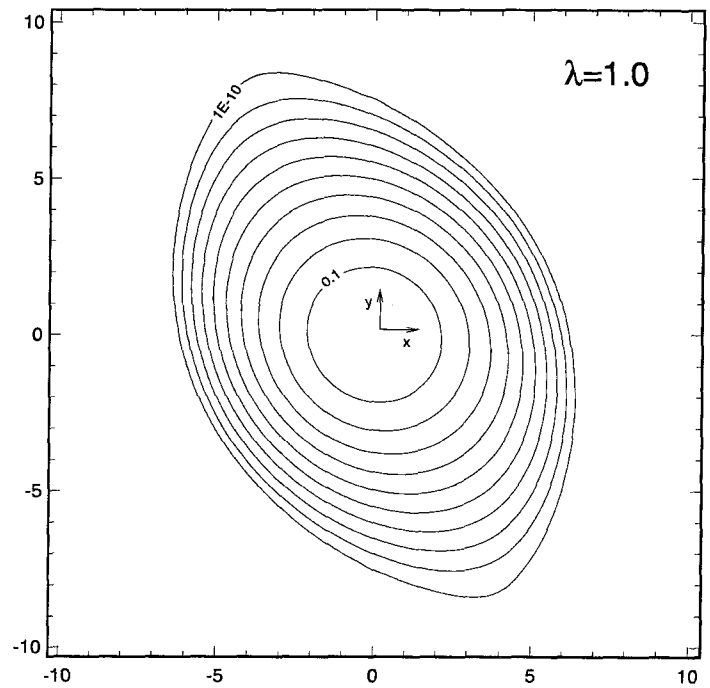

Figure 2.15: Isovorticity contours for $R = 100$, $\lambda = 1.0$, $M, N = 40$. This case corresponds to a confined vorticity solution in plane strain.

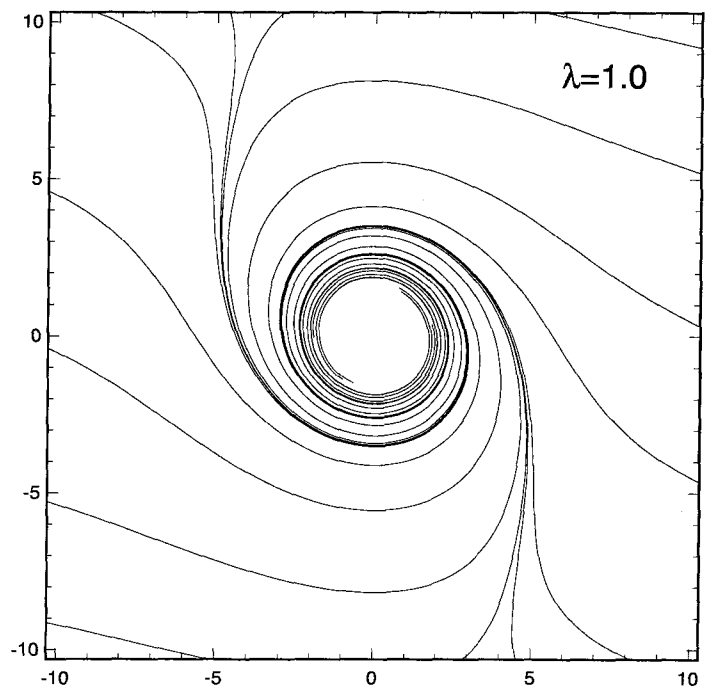

Figure 2.16: Projected Streamlines for $R = 100$, $\lambda = 1.0$, $M, N = 40$.

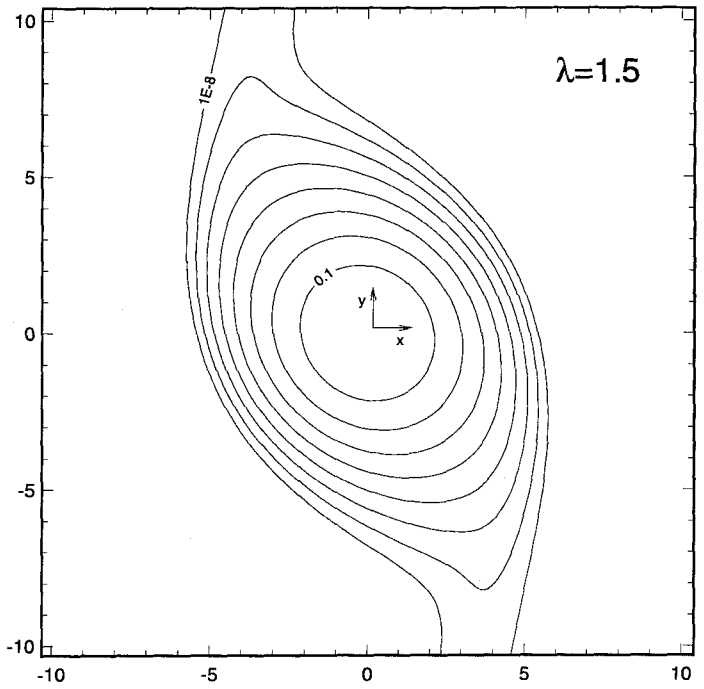

Figure 2.17: Isovorticity contours for $R = 100$, $\lambda = 1.5$, $M, N = 40$.

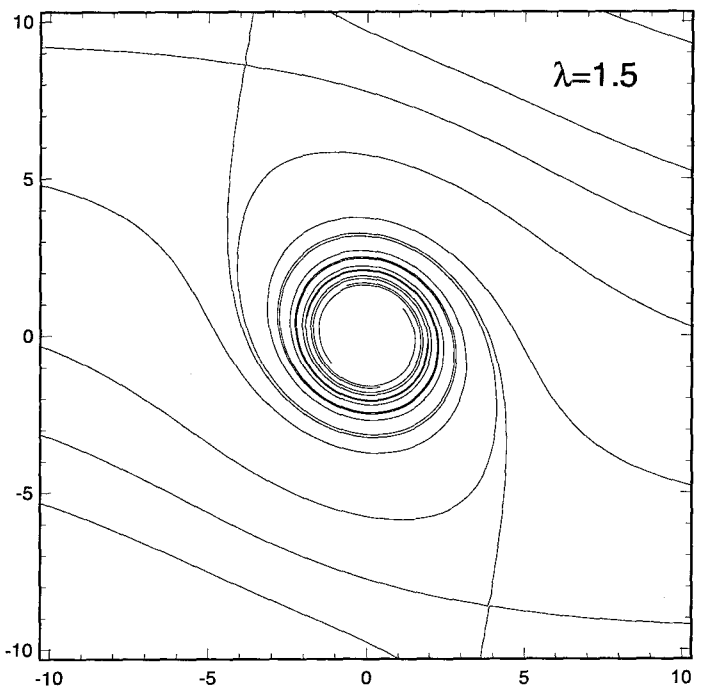

Figure 2.18: Projected Streamlines for $R = 100$, $\lambda = 1.5$, $M, N = 40$. Stagnation points appear at $x = \pm 3.8, y = \mp 8.6$.

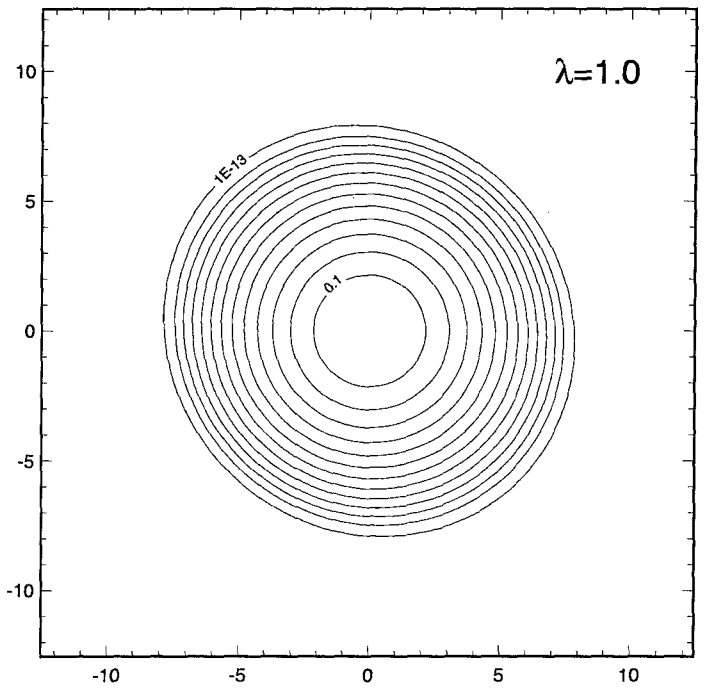

Figure 2.19: Isovorticity contours for $R = 1000$, $\lambda = 1.0$, $M, N = 50$.

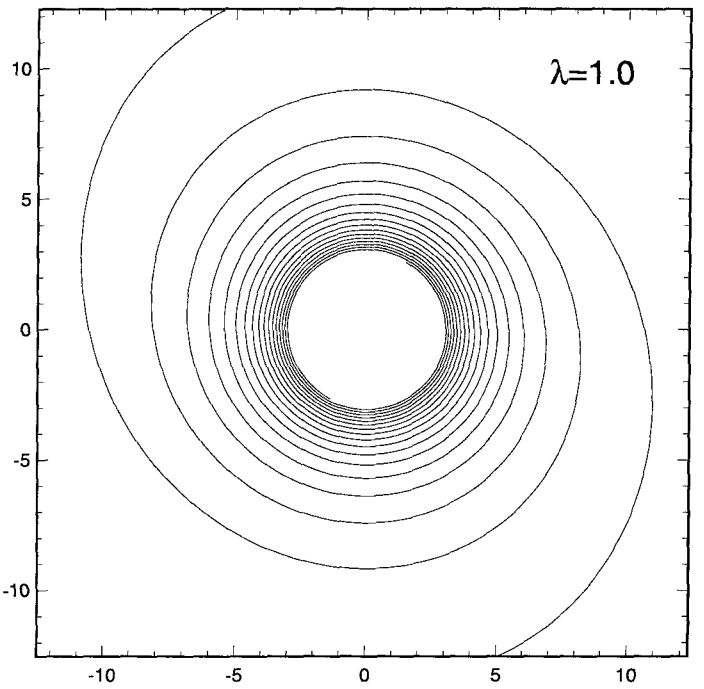

Figure 2.20: Projected Streamlines for $R = 1000$, $\lambda = 1.0$, $M, N = 50$.

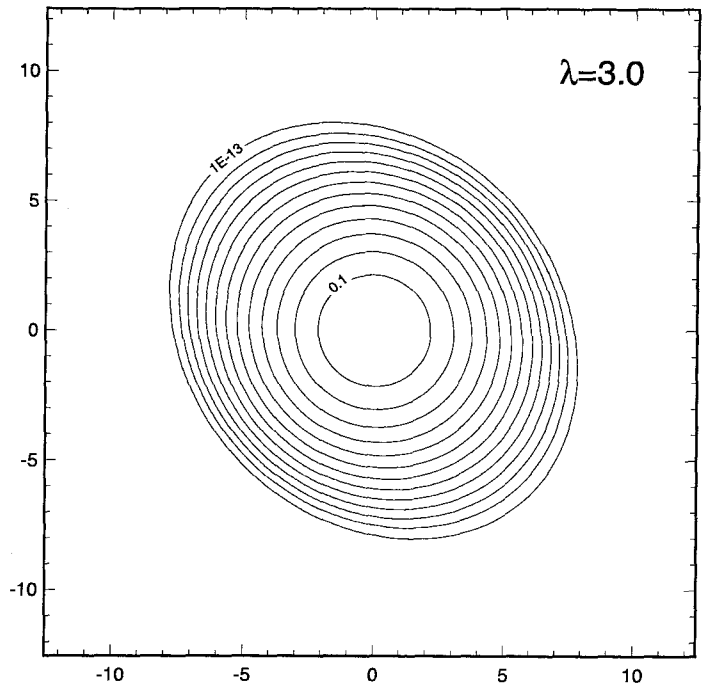

Figure 2.21: Isovorticity contours for $R = 1000$, $\lambda = 3.0$, $M, N = 50$.

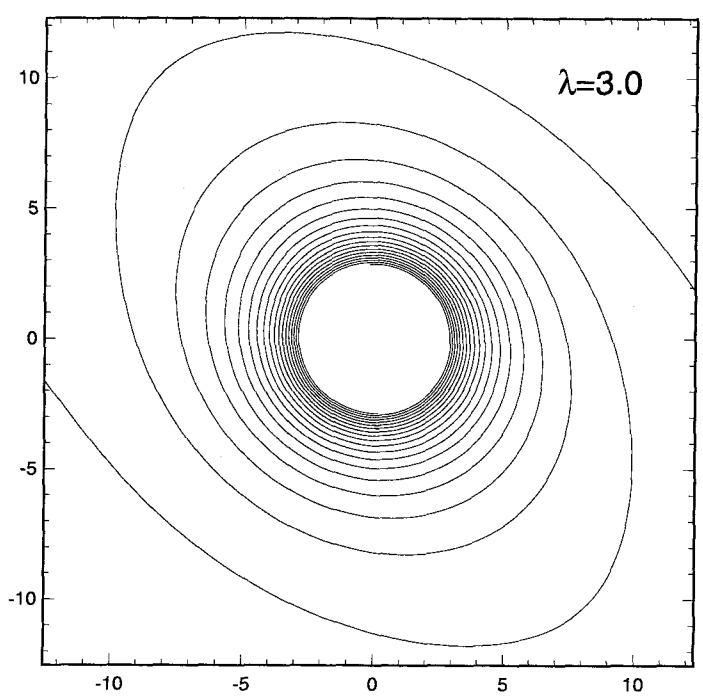

Figure 2.22: Projected Streamlines for $R = 1000$, $\lambda = 3.0$, $M, N = 50$.

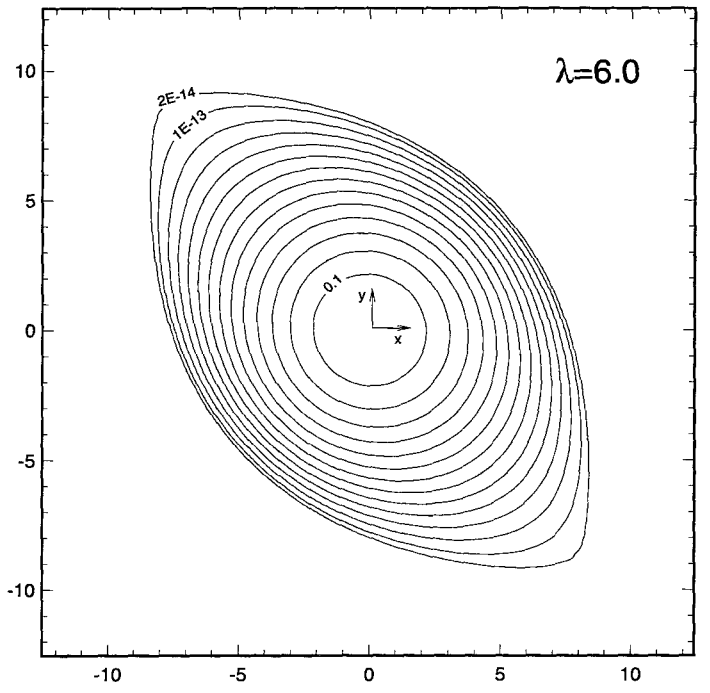

Figure 2.23: Isovorticity contours for $R = 1000$, $\lambda = 6.0$, $M, N = 50$.

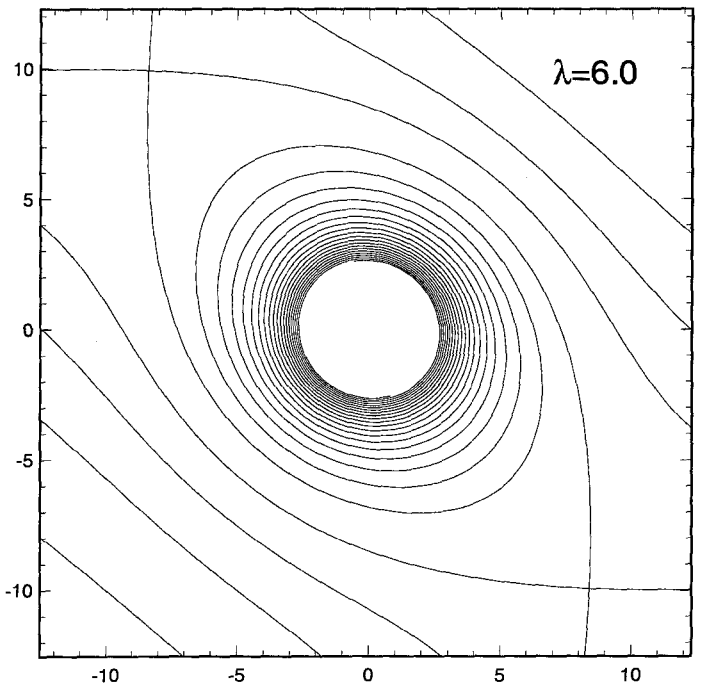

Figure 2.24: Projected Streamlines for $R = 1000$, $\lambda = 6.0$, $M, N = 50$. Stagnation points appear at $x = \pm 8.6, y = \mp 10.0$.

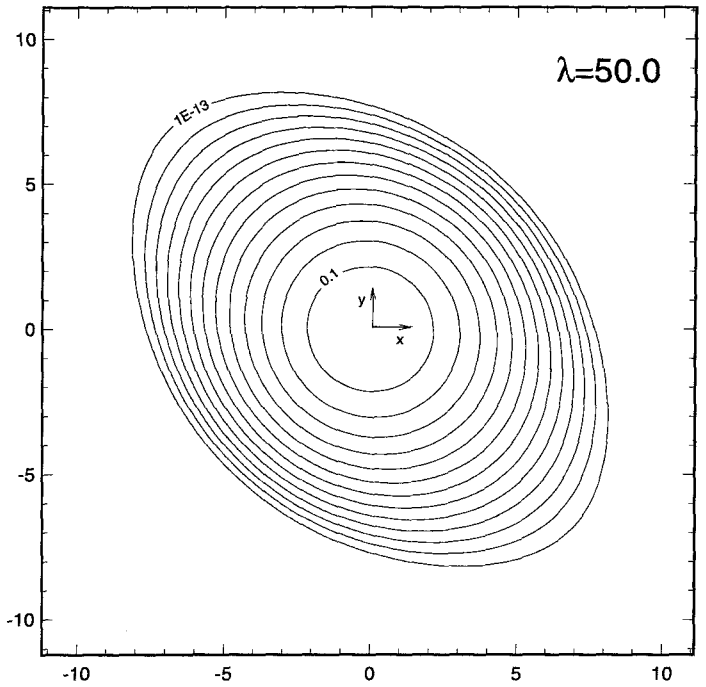

Figure 2.25: Isovorticity contours for $R = 10,000$, $\lambda = 50.0$, $M, N = 50$.

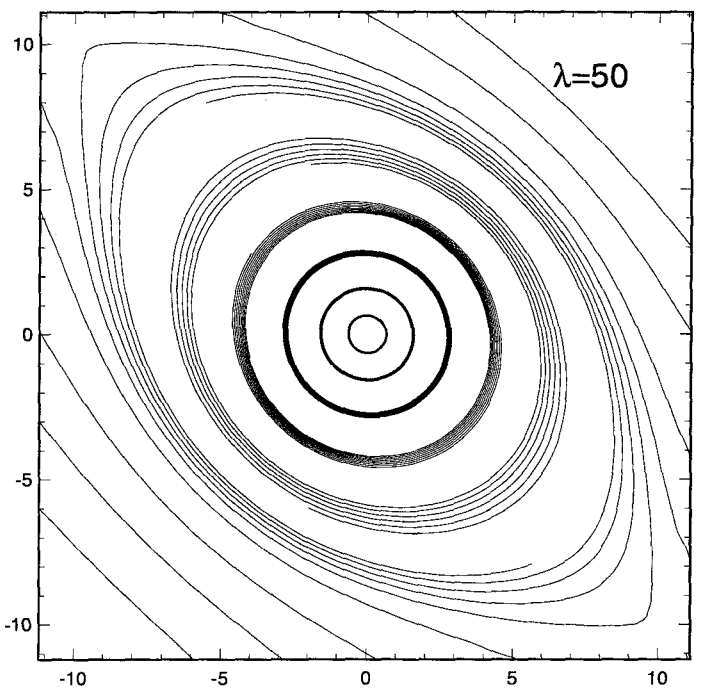

Figure 2.26: Projected Streamlines for $R = 10,000$, $\lambda = 50.0$, $M, N = 50$. Stagnation points appear at $x = \pm 10.0, y = \mp 10.0$.

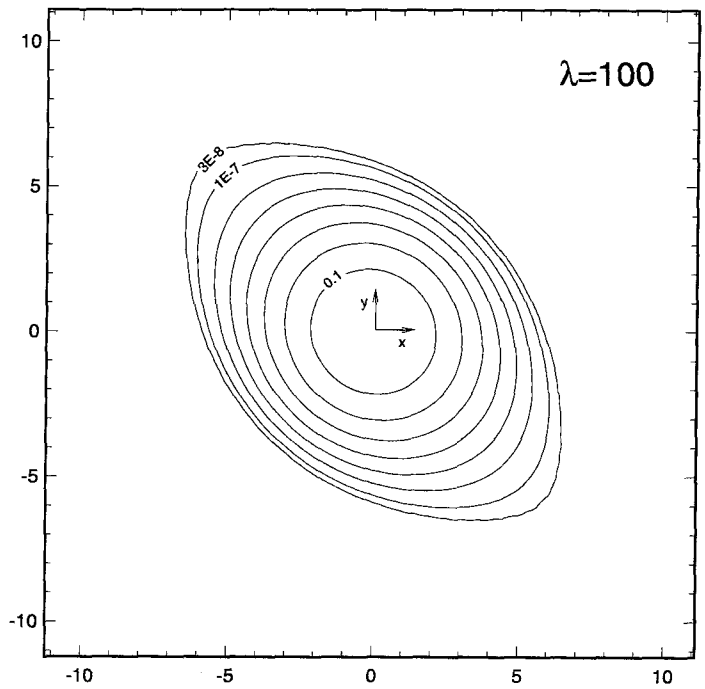

Figure 2.27: Isovorticity contours for $R = 10,000$, $\lambda = 100$, $M, N = 50$.

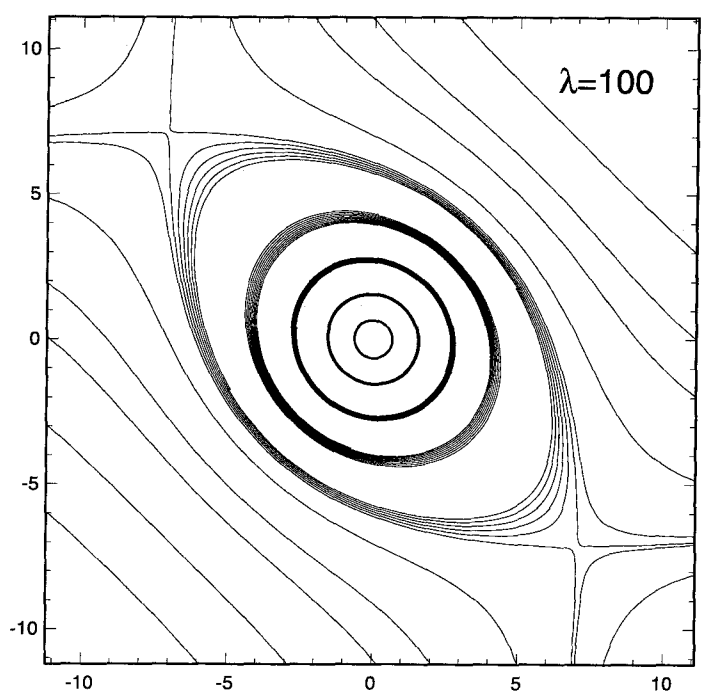

Figure 2.28: Projected Streamlines for $R = 10,000$, $\lambda = 100$, $M, N = 50$. Stagnation points appear at $x = \pm 7.1, y = \mp 7.1$.

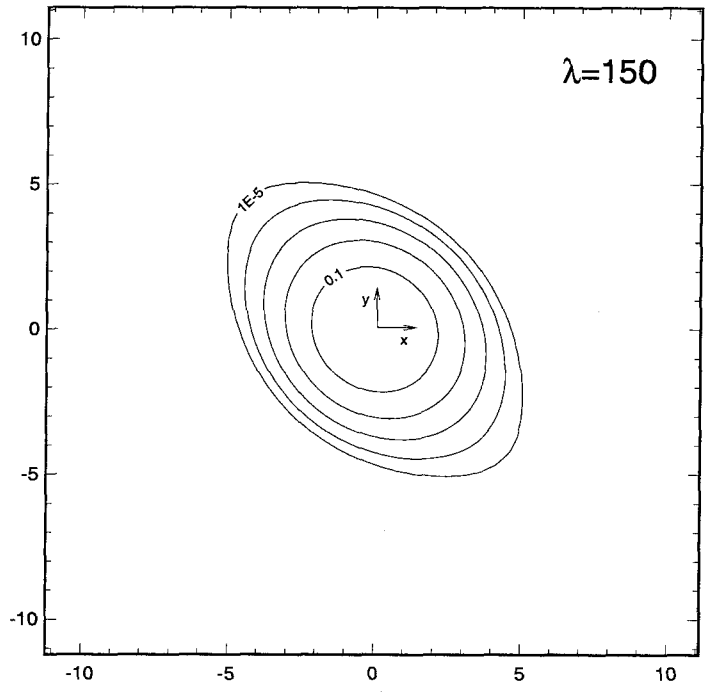

Figure 2.29: Isovorticity contours for $R = 10,000$, $\lambda = 150$, $M, N = 50$.

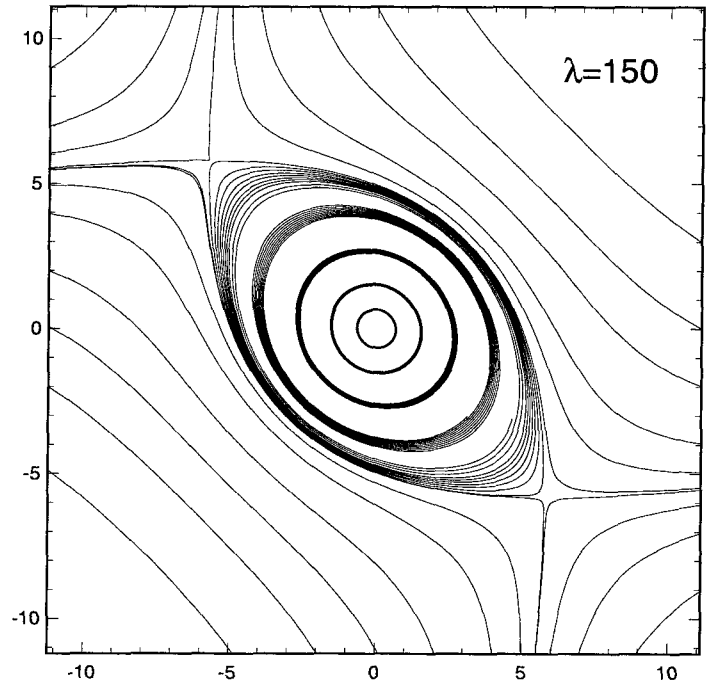

Figure 2.30: Projected Streamlines for $R = 10,000$, $\lambda = 150$, $M, N = 50$. Stagnation points appear at $x = \pm 5.8, y = \mp 5.8$.

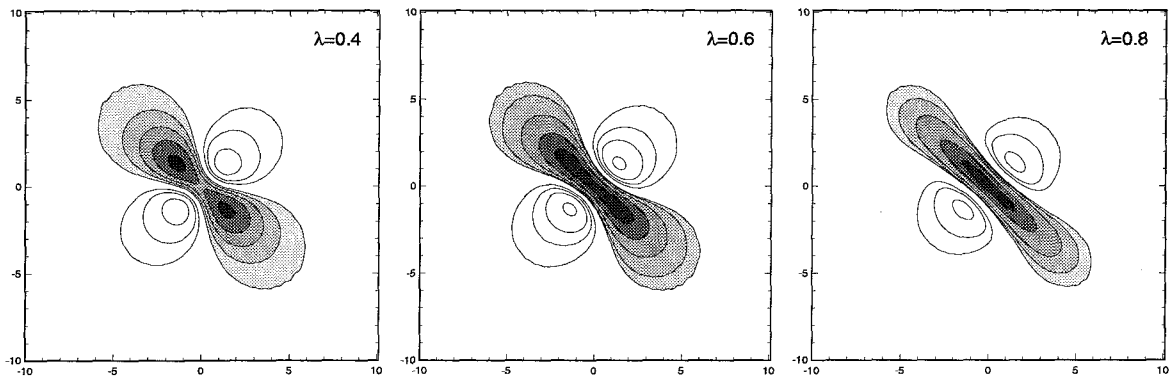

Figure 2.31: Dissipation contours at $R = 1$, $\lambda = 0.4, 0.6, 0.8$.

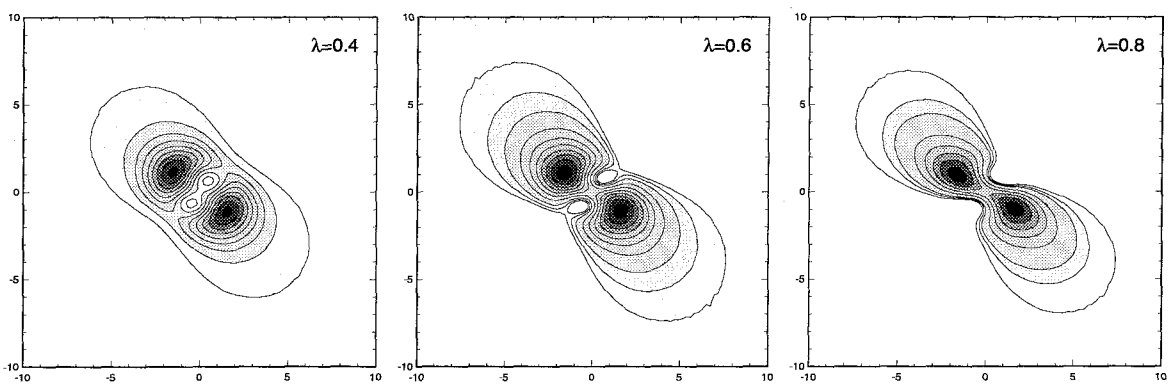

Figure 2.32: Dissipation contours at $R = 10$, $\lambda = 0.4, 0.6, 0.8$.

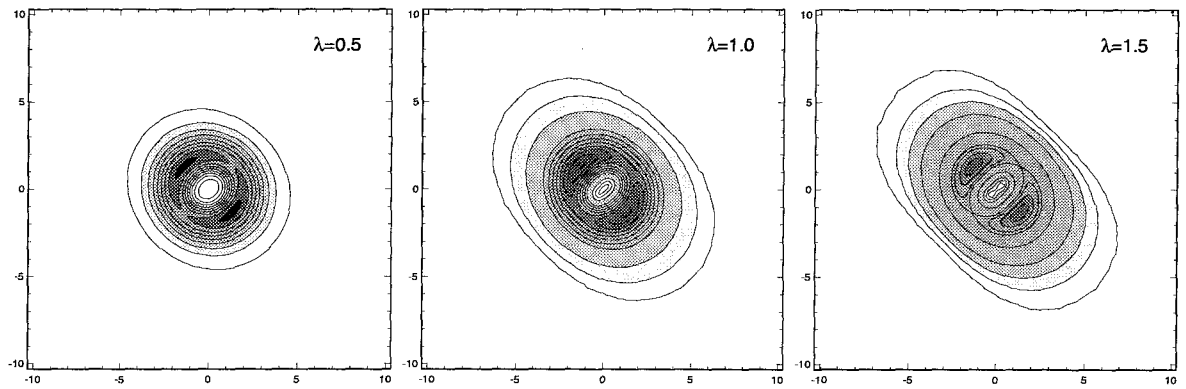

Figure 2.33: Dissipation contours at $R = 100$, $\lambda = 0.5, 1.0, 1.5$.

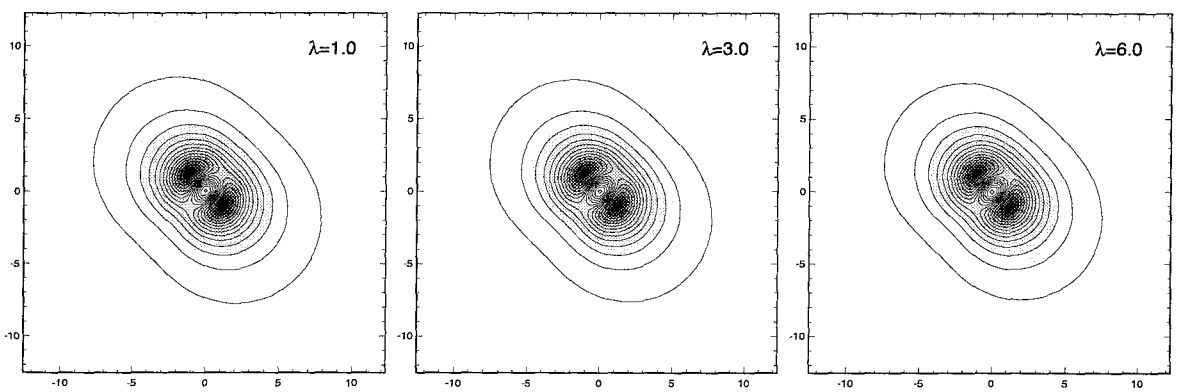

Figure 2.34: Dissipation contours at $R = 1000$, $\lambda = 1.0, 3.0, 6.0$.

Chapter 3 Biaxial Strain at Large Reynolds Number

3.1 Characteristic regions of the flow

We observe from our numerical results that for $R \gg 1$ the vortex becomes increasingly circular which makes the axisymmetric Burgers vortex a very good approximation the flow until the strain ratio becomes large enough such that outside of the core of the vortex, the isovorticity contours resemble Figure 3.1. This figure shows several key characteristic regions of the flow. Region I, the core of the vortex, within $r = O(1)$, is where viscous diffusion of vorticity is balanced by the intensification of vorticity by vortex stretching, and the streamlines and isovorticity contours are nearly circular. Region II, which we will call the *cat's-eye*, due to its shape, is defined as the interior region between the stagnation points of the flow, $1 < r < \varepsilon^{-1/2}$, when the strain ratio is large, $\lambda \gg 1$, the Reynolds number is large, $R \gg 1$, but their ratio is small,

$$\varepsilon \equiv \frac{\lambda}{R} \ll 1. \tag{3.1}$$

In this region, the vorticity is exponentially small and is basically convected along streamlines. The flow in the x-y plane is almost two-dimensional. The cat's-eye shape will accurately describe the contours of the vorticity and almost describe the streamlines, as shown, for example, in Figures 2.23–2.30. The velocity in this region is dominated by the core vorticity and the external strain. Region III begins at each stagnation point and extends away from the vortex. Vorticity in this region is also exponentially small, but it is convected away by the strain, which begins to dominate the induced velocities from the core. Region IV is the far field where structure of the vortex becomes unimportant.

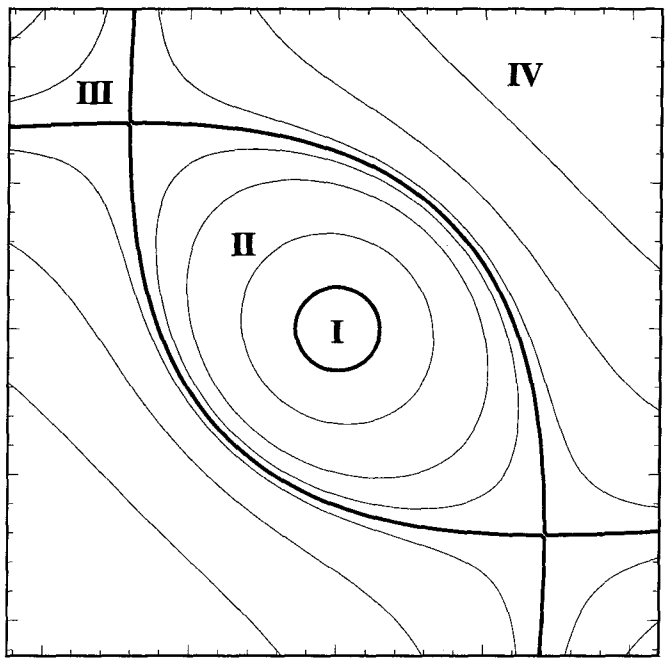

Figure 3.1: Schematic of the two-dimensional asymptotic limit of projected streamlines that divide the characteristic regions of the nearly two-dimensional flow for $\lambda \gg 1$, $R \gg 1$ and $\varepsilon \ll 1$.

We develop an asymptotic form for the vorticity in Region II and use this to determine the rate of decrease in circulation out of the cat's-eye. Then, we consider the nature of the vorticity leakage through Region III and match the rate of circulation increase in Region IV to the flux of vorticity from the cat's-eye.

3.2 Region II, the cat's-eye

3.2.1 Derivation of vorticity

We can write the nondimensional vorticity equation (2.1) in its steady form in two parts by considering the strain to consist of the sum of an axially symmetric three-dimensional part and a two-dimensional pure strain part,

$$L_1(\omega) + L_2(\omega) = 0, \tag{3.2}$$

where

$$L_1(\omega) = \frac{\partial^2\omega}{\partial x^2} + \frac{\partial^2\omega}{\partial y^2} + x\frac{\partial\omega}{\partial x} + y\frac{\partial\omega}{\partial y} + 2\omega, \tag{3.3}$$

$$L_2(\omega) = (\lambda x - Ru)\frac{\partial\omega}{\partial x} + (-\lambda y - Rv)\frac{\partial\omega}{\partial y}. \tag{3.4}$$

Notice that the terms of L_1 represent the balance of viscous diffusion of vorticity and intensification of vorticity by vortex stretching in an axisymmetric strain while the terms of L_2 correspond to the effective two-dimensional transport of vorticity by the induced velocity and two-dimensional, or in-plane, strain. Focusing first on L_2, we hypothesize that the flow in the region outside the core of the vortex, $r > 1$, can be represented to leading order by the potential flow of a point vortex in the pure two-dimensional strain. The streamfunction and velocity for this potential flow can be written as

$$\psi_0(x,y) = -\ln\sqrt{x^2+y^2} - \varepsilon xy, \tag{3.5}$$

$$u_x \equiv \frac{\partial\psi_0}{\partial y} = -\frac{y}{x^2+y^2} - \varepsilon x, \tag{3.6}$$

$$u_y \equiv -\frac{\partial\psi_0}{\partial x} = \frac{x}{x^2+y^2} + \varepsilon y. \tag{3.7}$$

The stagnation points of this flow occur where the velocities induced by the point vortex and the strain balance,

$$x_s = \pm\sqrt{\frac{1}{2\varepsilon}}, \tag{3.8}$$

$$y_s = \mp\sqrt{\frac{1}{2\varepsilon}}, \tag{3.9}$$

or, in polar coordinates,

$$r_s = \varepsilon^{-\frac{1}{2}}, \qquad \theta = \frac{3\pi}{4}, -\frac{\pi}{4}. \tag{3.10}$$

The true projected streamlines for the numerical solutions of Chapter 2 show a near cat's-eye form where λ and R are given by (3.1), as can be seen in Figures 2.25–2.29.

Note that, for the full three-dimensional straining field, the in-plane velocities will balance at

$$x_s = \pm\left(\frac{\lambda-1}{\lambda+1}\right)^{\frac{1}{4}}\sqrt{\frac{1}{2\varepsilon}}, \tag{3.11}$$

$$y_s = \mp\left(\frac{\lambda+1}{\lambda-1}\right)^{\frac{1}{4}}\sqrt{\frac{1}{2\varepsilon}}, \tag{3.12}$$

or, in polar coordinates,

$$r_s = \left(\frac{\lambda^2}{\lambda^2-1}\right)^{\frac{1}{4}}\varepsilon^{-\frac{1}{2}}, \qquad \theta = \frac{3\pi}{4}, -\frac{\pi}{4}, \tag{3.13}$$

so that comparison with (3.10) will require that λ be large.

The full streamfunction for the two-dimensional component of the velocities is rewritten in the form,

$$\psi = \psi_0 + \psi_1, \tag{3.14}$$

$$\nabla^2\psi = \nabla^2\psi_1 = -\omega. \tag{3.15}$$

The higher order correction, ψ_1, can be decomposed into two parts. First, we know from the MKO94 inner solution that the flow in the core is not perfectly circular like the Burgers vortex and there will be a streamfunction associated with the ellipticity. Second, there will be a streamfunction associated with the exponentially small velocity induced by vorticity outside of the core. When (3.14) is used in (3.2), the vorticity equation becomes

$$L_1(\omega) + L_3(\omega) + L_4(\omega) = 0, \tag{3.16}$$

$$L_1(\omega) = \frac{\partial^2\omega}{\partial x^2} + \frac{\partial^2\omega}{\partial y^2} + x\frac{\partial\omega}{\partial x} + y\frac{\partial\omega}{\partial y} + 2\omega, \tag{3.17}$$

$$L_3(\omega) = R\left(\frac{\partial\psi_0}{\partial y}\frac{\partial\omega}{\partial x} - \frac{\partial\psi_0}{\partial x}\frac{\partial\omega}{\partial y}\right), \tag{3.18}$$

$$L_4(\omega) = R\left(\frac{\partial\psi_1}{\partial y}\frac{\partial\omega}{\partial x} - \frac{\partial\psi_1}{\partial x}\frac{\partial\omega}{\partial y}\right). \tag{3.19}$$

For large R, when $1 < r < \varepsilon^{-1/2}$, we argue that both ω and ψ_1 will be exponentially small , with the consequence that the dominant terms of the equation will be $L_3(\omega)$. Solving $L_3(\omega) = 0$ will require that

$$\omega = \omega(\psi_0) = \omega\left(-\ln\sqrt{x^2+y^2} - \varepsilon xy\right). \tag{3.20}$$

Of the remaining terms, owing to what we will now show to be exponentially small vorticity in region II, those of L_1 will be dominant over those of L_4. If we consider solving $L_1(\omega) = 0$, the solution will have the property that an average around a circle of radius $r = \sqrt{x^2+y^2}$, should have the form of Burgers vortex,

$$\frac{1}{2\pi}\int \omega d\theta = e^{-r^2/2} = e^{-\frac{1}{2}\left(x^2+y^2\right)}. \tag{3.21}$$

Satisfying both of these requirements, we find that the vorticity must take the form,

$$\omega_{\mathrm{II}}(x,y) = R\exp\left[-\frac{1}{2}\exp\left(-2\psi_0\right)\right] = Re^{-\frac{1}{2}\left(x^2+y^2\right)\exp(2\varepsilon xy)}, \tag{3.22}$$

or, in polar coordinates,

$$\omega_{\mathrm{II}}(r,\theta) = Re^{-\frac{r^2}{2}\exp(\varepsilon r^2\sin 2\theta)} \tag{3.23}$$

within the cat's-eye region. It may be verified by direct substitution of (3.5) and (3.22) into (3.18), that $L_3(\omega) = 0$ is satisfied. Expanding (3.22) in orders of ε,

$$\omega_{\mathrm{II}}(r,\theta) = Re^{-r^2/2}\left[1 - (\varepsilon\sin 2\theta)\frac{r^4}{2} + O\left(\varepsilon^2\right)\right]. \tag{3.24}$$

which matches, when $r \to 0$, to the MKO94 asymptotic solution for $R \gg 1$, (in terms of their scaling definitions)

$$\omega = \omega_0 + \varepsilon\Omega(r)\sin 2\theta + O\left(\varepsilon^2\right), \tag{3.25}$$

$$\Omega(r) \sim \frac{1}{16}r^4 e^{-r^2/4} \tag{3.26}$$

as $r \to \infty$. In order to remedy the disordering of terms of the the MKO94 solution at $r = (2/\varepsilon)^{1/4}$, Jiménez *et al.* [7] performed an asymptotic analysis involving the Lundgren transformation and coordinate stretching that delayed the disordering to $r = \varepsilon^{-1/2}$, (again in terms of their definitions, which involve time dependence due to the Lundgren transformation),

$$\omega(R,\theta) = \frac{1}{4\pi t} e^{-R^2/4t} + O\left(\varepsilon^2\right), \tag{3.27}$$

where, in their notation, $R = \hat{r} - \varepsilon \hat{r}^3 \pi \sin 2\theta$. Again, (3.23) matches their form to $O(\varepsilon^2)$. Figures 3.2–3.3 show that the agreement between (3.22) and numerics for $R = 1000$, $\lambda = 50, 100$ is excellent. The vorticity at the stagnation point (and at any point along the cat's-eye boundary) given by (3.22) is $\omega_s = \exp(-1/2e\varepsilon)$. This value is compared to numerics in Table 3.1 for cases in which the stagnation point appears within the domain of valid of the steady calculation. The stagnation point is used because it appears at the limit of the region of the validity of (3.22), yet the agreement is still very good.

Table 3.1: Stagnation point vorticity

R	λ	ω_{II}	ω_{numerics}
1,000	6.0	1.02E-14	4.85E-14
10,000	100	9.89E-9	1.03E-8
10,000	150	1.29E-6	4.72E-6

A comparison of (3.23) with the asymptotic formulations from MKO94 (3.25), Jiménez *et al.* [7] (3.27), and the present numerical solutions along cuts $\theta = \pi/4$ and $\theta = -\pi/4$ are shown in Figures 3.4–3.5 respectively. Along $\theta = \pi/4$, all theories give good agreement to the numerics except MKO94 which changes sign at $r \approx 3.76$ and therefore becomes infinitely negative on the log scale. Along $\theta = -\pi/4$, Figure 3.5 clearly shows that (3.23) is the only form that is accurate to the edge of the cat's-eye. The isovorticity contours of the various asymptotic formulations are shown in Figures 3.6–3.8 for comparison.

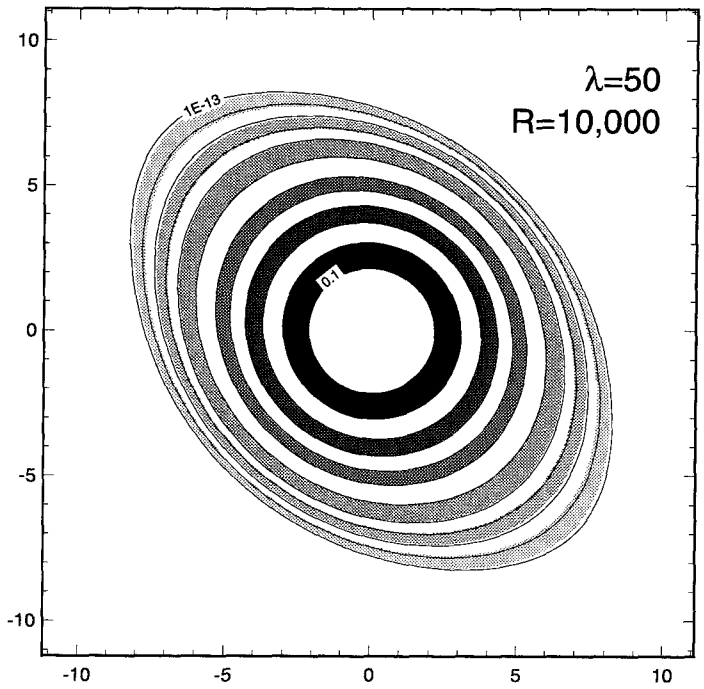

Figure 3.2: Comparison of isovorticity contours of numerical results (shaded regions) to Equation (3.22) (solid lines) for $R = 10,000$, $\lambda = 50$.

3.2.2 Streamfunction calculation

We now calculate the streamfunction associated with ω_{II} from (3.14) and (3.23),

$$\nabla^2 \psi_1 = -\omega_{\text{II}}/R = -e^{-\frac{r^2}{2}\exp(\varepsilon r^2 \sin 2\theta)}, \tag{3.28}$$

which was solved by considering

$$\psi_1 = e^{-\frac{r^2}{2}\exp(\varepsilon r^2 \sin 2\theta)} \left[F_1(r) + \varepsilon F_2(r) \sin 2\theta + \cdots\right]. \tag{3.29}$$

The resulting equation for F_1 is

$$F_1'' + \left(\frac{1}{r} - 2r\right) F_1' + \left(r^2 - 1\right) F_1 = 1 \tag{3.30}$$

which is solved using variation of parameters of the homogeneous solutions, $e^{-r^2/2}$, $\ln r e^{-r^2/2}$, and we find,

$$F_1(r) = \frac{1}{2}\,\text{Ei}\left(\frac{-r^2}{2}\right) e^{r^2/2}. \tag{3.31}$$

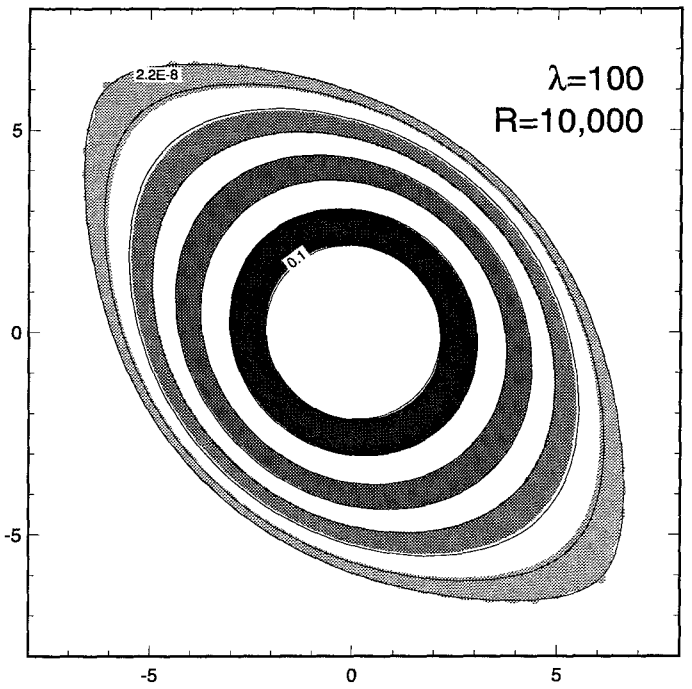

Figure 3.3: Comparison of isovorticity contours of numerical results (shaded regions) to Equation (3.22) (solid lines) for $R = 10,000$, $\lambda = 100$.

Then, this solution forces the equation for F_2,

$$F_2'' + \left(\frac{1}{r} - 2r\right) F_2' + \left(r^2 - \frac{4}{r^2} - 2\right) F_2 = 4r^2 + 3r^2 \,\mathrm{Ei}\left(\frac{-r^2}{2}\right) e^{r^2/2}, \tag{3.32}$$

which is also solved by various of parameters of the homogeneous solutions, $r^{\pm 2} e^{r^2/2}$. Then, using the boundary condition that $F_2 \to 0$ as $r \to 0$, we find,

$$F_2(r,\theta) = -\frac{r^4}{4} \,\mathrm{Ei}\left(\frac{-r^2}{2}\right) e^{r^2/2} \sin 2\theta + \frac{6 \sin 2\theta}{r^2}\left(1 + \frac{r^2}{2} + \frac{r^4}{12} - e^{-r^2/2}\right). \tag{3.33}$$

Realizing that the coefficient of the exponential integral, Ei, is $(1 - \varepsilon r^4 \sin 2\theta/2)\, e^{r^2/2}$, *i.e.* the leading terms of an epsilon expansion of $\frac{1}{2} e^{r^2/2 \exp(\varepsilon r^2 \sin 2\theta)}$, and matching to the Burgers vortex as $r \to 0$ yields

$$\begin{aligned} \psi_1 \;=\; & \frac{1}{2} E_1\left(\frac{-r^2}{2}\right) \\ & + \varepsilon \frac{6 \sin 2\theta}{r^2}\left(1 + \frac{r^2}{2} + \frac{r^4}{12} - e^{-r^2/2}\right) e^{-\frac{r^2}{2} \exp(\varepsilon r^2 \sin 2\theta)} + O\left(\varepsilon^2\right), \end{aligned} \tag{3.34}$$

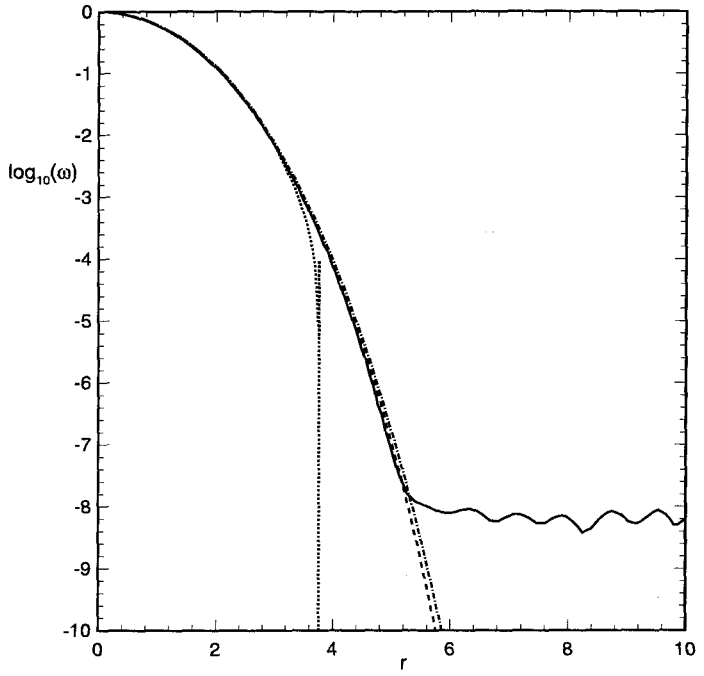

Figure 3.4: Vorticity along $\theta = \pi/4$ from MKO94 (3.25) (dotted), JMV96 (3.27) (dash-dot), our result, (3.23) (dashed), and numerics (solid) for $\lambda = 100$, $R = 10,000$, $\varepsilon = 0.01$. Note that the MKO94 result becomes disordered and negative, so that the log blows up at $r = 3.76$.

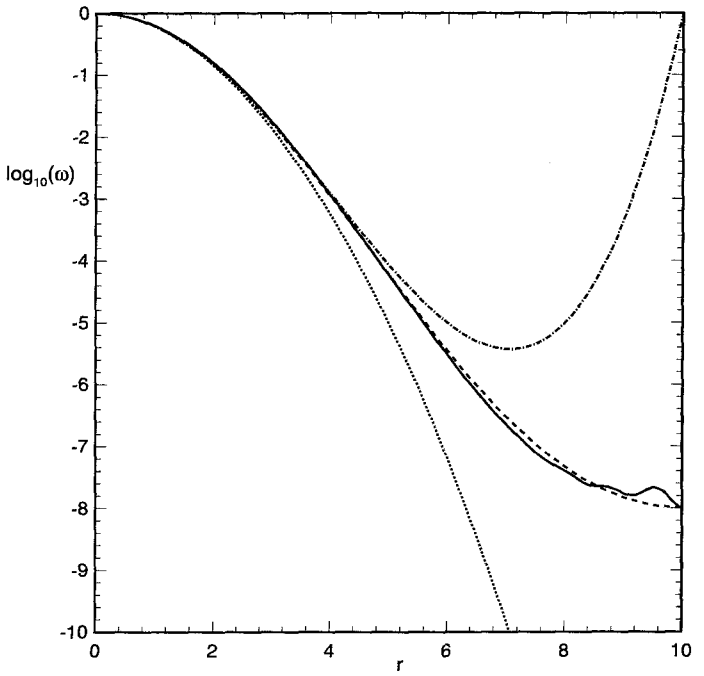

Figure 3.5: Vorticity along $\theta = -\pi/4$ from MKO94 (3.25) (dotted), JMV96 (3.27) (dash-dot), our result, (3.23) (dashed), and numerics (solid) for $\lambda = 100$, $R = 10,000$, $\varepsilon = 0.01$.

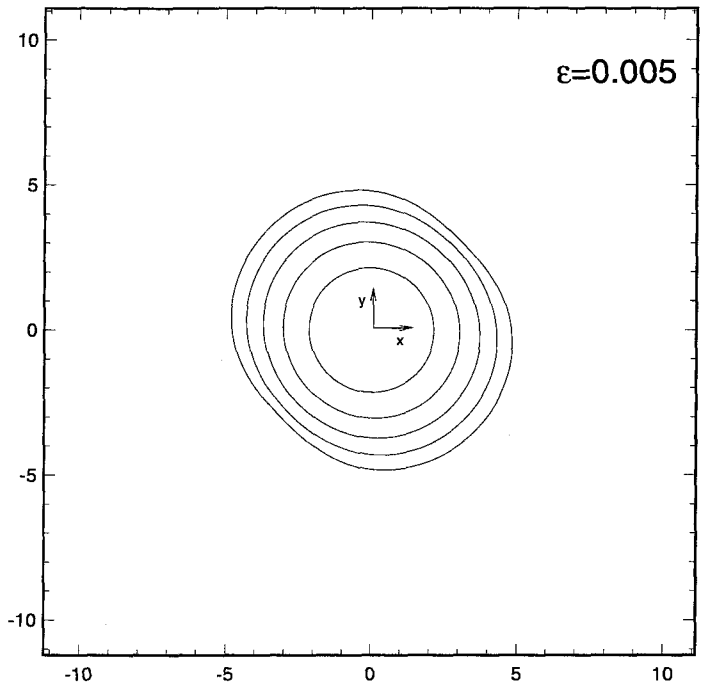

Figure 3.6: Isovorticity contours of MKO94 asymptotic analysis, equation (3.25), for $\varepsilon = 0.005$.

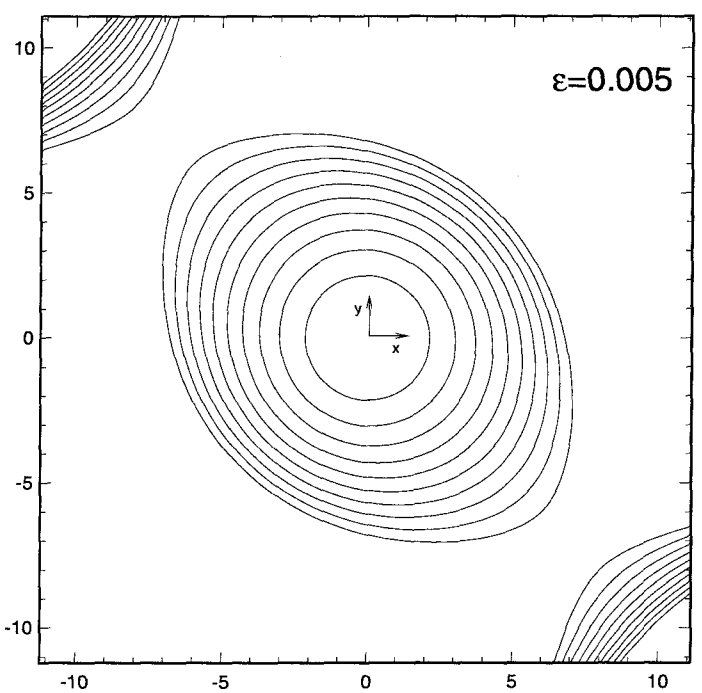

Figure 3.7: Isovorticity contours of JMV96 asymptotic analysis, equation (3.27), for $\varepsilon = 0.005$.

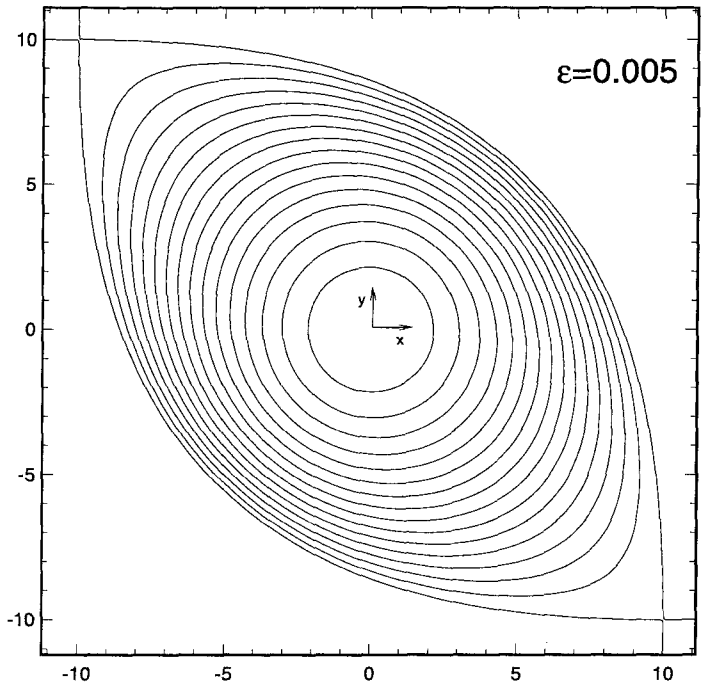

Figure 3.8: Isovorticity contours of equation (3.23) for $\varepsilon = 0.005$.

where $E_1\left(\frac{-r^2}{2}\right)$ is another form of the exponential integral, as defined by Abramowicz and Stegun [1],

$$E_1(z) = \int_0^z \frac{1-e^{-t}}{t} dt - \ln z - \gamma, \tag{3.35}$$

where γ is Euler's constant. Thus, we have found that the corrections to the stream-function in the Region II are exponentially small and therefore the terms of L_4 are small compared to L_1, and both are exponentially smaller than the terms of L_3.

3.2.3 Summary and Generalization

In Region II, the essential properties of the flow are that the core of the vortex can be closely approximated by a point vortex and that the exponentially small vorticity is being convected by the background strain, which is composed of stretching and two-dimensional components. Since the two dimensional components of the strain and the point vortex can be represented by the potential flow (3.5), the vorticity can

be written in the form,

$$\omega_{\rm II} = R\exp\left[-\frac{1}{2}\exp\left(-2\psi_0\right)\right] = Re^{-\frac{r^2}{2}\exp(\varepsilon r^2\sin 2\theta)}. \tag{3.36}$$

The associated streamfunction for the flow may be represented as,

$$\begin{aligned}
\psi &= \psi_{\rm BV} + \psi_{\rm strain} + \psi_{\rm II}, && (3.37)\\
\psi_{\rm BV} &= -\int_0^r \left(1 - e^{-\rho^2/2}\right)\frac{1}{\rho}d\rho, && (3.38)\\
\psi_{\rm strain} &= -\varepsilon r^2\sin 2\theta, && (3.39)\\
\psi_{\rm II} &= \varepsilon\frac{6\sin 2\theta}{r^2}\left(1 + \frac{r^2}{2} + \frac{r^4}{12} - e^{-r^2/2}\right)e^{-\frac{r^2}{2}\exp(\varepsilon r^2\sin 2\theta)} + O\left(\varepsilon^2\right). && (3.40)
\end{aligned}$$

It is interesting to note that this approach is not limited to the case of biaxial strain. For instance, given the Burgers vortex embedded in a strain field in which the two-dimensional component can be written as the streamfunction, $\psi_{\rm general} = \lambda_n r^n \sin n\theta$, $n > 1$, where λ_n is a measure of the strength of the strain field, its asymptotic form outside of the vortex core but within some dividing streamline will be, for $\varepsilon_n = \lambda_n/R$,

$$\begin{aligned}
\omega &= R\exp\left[-\frac{r^2}{2}\exp\left(-2\varepsilon_n r^n\sin n\theta\right)\right], && (3.41)\\
\psi &= -\int_0^r \left(1 - e^{-\rho^2/2}\right)\frac{1}{\rho}d\rho + \varepsilon_n r^n\sin n\theta + \psi_1 + O(\varepsilon_n^2), && (3.42)\\
\nabla^2\psi_1 &= -\omega/R. && (3.43)
\end{aligned}$$

The cat's-eye shape corresponds to $n = 2$, and two other examples for $n = 3$ and $n = 4$ are shown in Figures 3.9–3.10 where the asymptotic form of the vortex exhibits triangular and square dividing streamlines, respectively. Clearly, for $\psi_{\rm general}$, the dividing streamline corresponds to an n-sided polygon at a radius of $\varepsilon_n^{-1/n}$ from the origin. It should be noted that for each case, the asymptotic form of the vortex core (Region I) could be calculated in a manner analogous to MKO94.

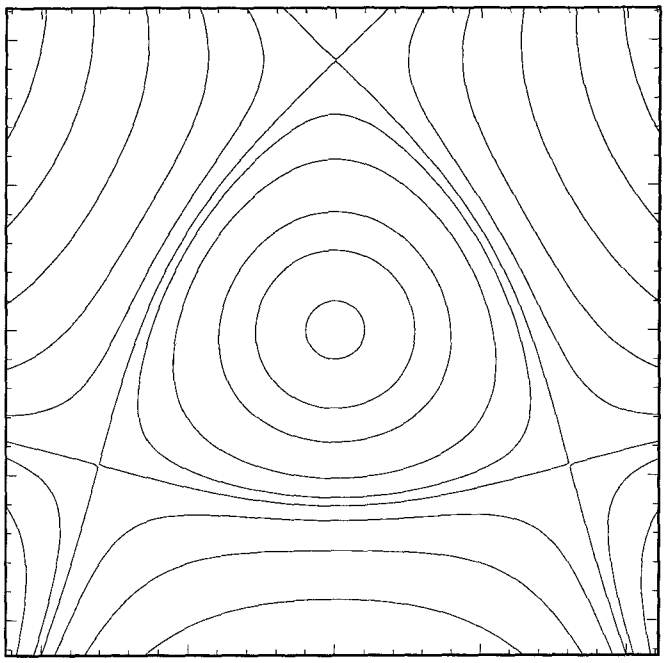

Figure 3.9: Asymptotic limit of the Burgers vortex in a straining field where $\psi_{general}(r,\theta) = r^3 \sin 3\theta$.

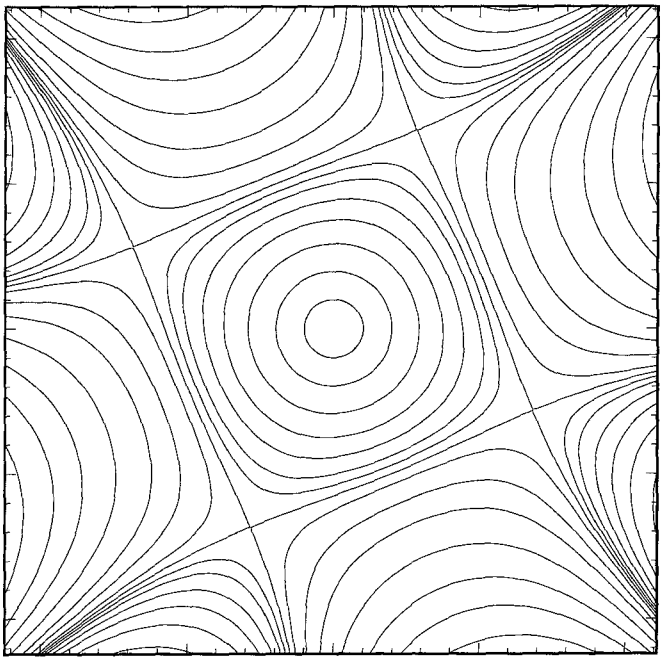

Figure 3.10: Asymptotic limit of the Burgers vortex in a straining field where $\psi_{general}(r,\theta) = r^4 \sin 4\theta$.

3.3 Slow decay of vortex for $\lambda \gg 1$

Although the solutions we are finding are nearly steady, in fact, numerically steady, there is extremely slow time variation in the form of flux of vorticity to infinity. This slow time variation was originally noted in MKO94 where they hypothesized that, in biaxial strain, diffusion would not be able to balance the strain. We perform a circulation decay rate estimate by considering flux of vorticity across the cat's-eye boundary and then analyze the structure of vorticity leaking into Region IV.

3.3.1 Flux of vorticity out of the cat's-eye

By integrating the dimensionless vorticity equation (2.1) over an area, A, and using the Green's theorem to relate area integrals to contour integrals, the time derivative of the circulation is easily found to be the sum of diffusion of vorticity and transport of vorticity across the boundary of the domain,

$$\frac{\partial \Gamma}{\partial t} \equiv \frac{\partial}{\partial t} \iint_A \omega dA = \underbrace{\oint_{\partial A} (\nabla \omega \cdot \mathbf{n})\, dl}_{\text{Diffusion}} - \underbrace{\oint_{\partial A} (\mathbf{u} \cdot \mathbf{n})\, \omega dl}_{\text{Transport}}, \tag{3.44}$$

where $\mathbf{n}$ is an outward-facing unit vector normal to the boundary and $\mathbf{u}$ is the velocity at the boundary. It will be useful to write the velocity decomposed into a two-dimensional part induced by vorticity and pure two-dimensional strain and a part associated with stretching,

$$\mathbf{u} = \mathbf{u}_1 + \mathbf{u}_2 = \begin{pmatrix} +\frac{\partial \psi}{\partial y} \\ -\frac{\partial \psi}{\partial x} \end{pmatrix} + \begin{pmatrix} -x \\ -y \end{pmatrix}. \tag{3.45}$$

If we choose the boundary A to be the edge of the cat's-eye, *i.e.* the contour defined by

$$\ln\left(\varepsilon(x^2+y^2)\right) + \varepsilon(x^2+y^2)\sin 2\theta = -1, \tag{3.46}$$

the dominant velocities will only come from $\psi \sim \psi_0(x,y) = -\ln\sqrt{x^2+y^2} - \varepsilon xy$, so that,

$$\mathbf{u} = \mathbf{u}_1 + \mathbf{u}_2 = \begin{pmatrix} +\frac{\partial\psi_0}{\partial y} \\ -\frac{\partial\psi_0}{\partial x} \end{pmatrix} + \begin{pmatrix} -x \\ -y \end{pmatrix}. \tag{3.47}$$

Along the cat's-eye, the unit normal vector is defined to be

$$\mathbf{n} = \frac{\nabla\psi_0}{(\nabla\psi_0 \cdot \nabla\psi_0)^{1/2}} = -\frac{\nabla\omega_{\text{II}}}{(\nabla\omega_{\text{II}} \cdot \nabla\omega_{\text{II}})^{1/2}} \tag{3.48}$$

$\mathbf{u}\cdot\mathbf{n}$ simplifies to,

$$\begin{aligned} \mathbf{u}\cdot\mathbf{n} &= \left(\frac{\partial\psi_0}{\partial y}\frac{\partial\psi_0}{\partial x} - \frac{\partial\psi_0}{\partial x}\frac{\partial\psi_0}{\partial y}\right) + \mathbf{u}_2\cdot\mathbf{n} \\ &= \mathbf{u}_2\cdot\mathbf{n}. \end{aligned} \tag{3.49}$$

Also, along this contour the cat's-eye vorticity from (3.22) is a constant, $\omega_c = R\exp(-1/2e\varepsilon)$, so with these simplifications we have

$$\frac{\partial\Gamma}{\partial t} = \omega_c \oint_{\partial A} \left(\frac{\nabla\omega_{\text{II}}}{\omega_c} - \mathbf{u}_2\right)\cdot\mathbf{n}dl. \tag{3.50}$$

Scaling r on $\varepsilon^{-1/2}$, $\rho = \varepsilon^{1/2}r$, and solving (3.46) for $\theta(\rho)$, we find that the circulation decrease in terms of dimensional variables is,

$$\frac{\partial\Gamma}{\partial t} = -\frac{c}{4\pi}\gamma\varepsilon^{-1}\Gamma\exp\left(\frac{-1}{2e\varepsilon}\right). \tag{3.51}$$

where c is defined by the integral along the cat's eye, in terms of ρ,

$$c = 4\int_m^1 \left(\frac{\nabla\omega_{\text{II}}(\rho)}{\omega_c} - \mathbf{u}_2(\rho)\right)\cdot\mathbf{n}(\rho)\sqrt{1+\rho^2\left(\frac{d\theta}{d\rho}\right)^2}\,d\rho. \tag{3.52}$$

where $m = 0.5276973963$ is found by solving (3.46) for $\theta = \pi/4$. Numerical integration of (3.52) results in $c = .48475$.

For comparison, MKO94 proposed a heuristic argument that the rate of reduction of circulation inside a circle of radius $\varepsilon^{-1/2}$ would be, in terms of the nondimension-

alization used in this thesis,

$$\frac{\partial \Gamma}{\partial t} \sim -\pi\beta\varepsilon^{-1}\Gamma \exp\left(-\frac{1}{2\varepsilon}\right). \tag{3.53}$$

Although the results look similar, our estimate of the circulation reduction is on the order of $\exp[(1/2e\varepsilon)(e-1)]$ greater than the MKO94 estimate, a very considerable amount for $\varepsilon \ll 1$. However, the circulation decay rate is still exponentially small and did not preclude us from finding the numerically steady solutions of Chapter 2.

This method of circulation decay rate calculation can be carried out for the generalized asymptotic solution (3.41). In general, the flux will be proportional to the vorticity on the dividing streamline and the length of the dividing streamline.

3.3.2 Structure of vorticity leakage into region IV

To determine the validity of our steady numerical results in the biaxial region, we use a time evolution code to examine how the vortices behave over time. It is found that the structure of the core of vortex persists over very long periods of time and that the effect of the biaxial strain is to strip away vorticity along a thin band on either side of the core, starting at the position of the stagnation point. This "tail" of leaking vorticity was only present for strain ratios in the biaxial region and for at least moderate Reynolds numbers of order 10^2. For lower circulation, biaxial strain will pull apart the vortex, but when the core of the vortex is close to circular, the tails appear.

We will now establish a working model for the structure of the tails. First we assume that, in this region, the induced velocities of the vortex are negligible compared to the local strain. Second, since the structure of the vorticity leakage at the cat's-eye is somewhat unknown, it will be approximated by a delta function at the boundary $y = 0$ and the coefficient of the delta function will be determined by matching the flux into region IV with the flux out of Region II. Assuming the velocities induced by the core of the vortex are small, the vorticity equation becomes

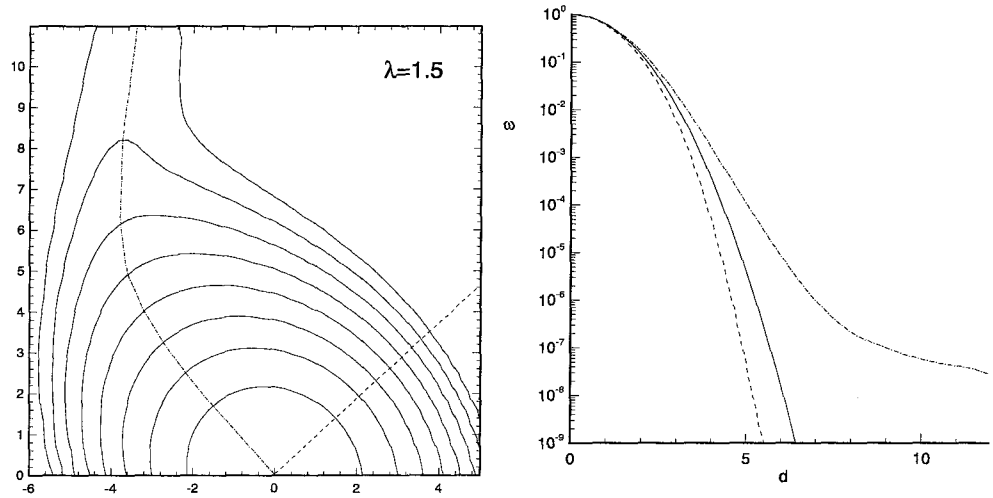

Figure 3.11: Vorticity along maximum (dashed) and minimum (dash dot) gradient lines at $R = 100$, $\lambda = 1.5$. The axisymmetric Burgers Vortex is shown for comparison with a solid line.

$$\frac{\partial \omega}{\partial t} - (1+\lambda)\, x \frac{\partial \omega}{\partial x} - (1-\lambda)\, y \frac{\partial \omega}{\partial y} = 2\omega + \frac{\partial^2 \omega}{\partial x^2} + \frac{\partial^2 \omega}{\partial y^2}. \tag{3.54}$$

Now, transforming the variables as follows,

$$\begin{aligned} X &= x e^{(1+\lambda)t}, \\ Y &= y e^{(1-\lambda)t}, \\ \Omega(X,Y,t) &= \omega(X e^{-(1+\lambda)t}, Y e^{-(1-\lambda)t}, t), \end{aligned} \tag{3.55}$$

yields

$$\frac{\partial \Omega}{\partial t} = 2\Omega + e^{2(1+\lambda)t} \frac{\partial^2 \Omega}{\partial X^2} + e^{2(1-\lambda)t} \frac{\partial^2 \Omega}{\partial Y^2}. \tag{3.56}$$

Taking the Fourier transform in X,

$$\begin{aligned} \tilde{\Omega}(k_1, Y, t) &= \frac{1}{2\pi} \int_{-\infty}^{\infty} \Omega e^{i k_1 X} dX, \\ \Omega(X, Y, t) &= \int_{-\infty}^{\infty} \tilde{\Omega} e^{-i k_1 X} dk_1, \end{aligned} \tag{3.57}$$

and then taking the Fourier sine transform in Y,

$$\begin{aligned} \hat{\Omega}(k_1, k_2, t) &= \frac{2}{\pi}\int_0^\infty \tilde{\Omega}\sin(k_2 Y)\, dY, \\ \tilde{\Omega}(k_1, Y, t) &= \int_0^\infty \hat{\Omega}\sin(k_2 Y)\, dk_2, \end{aligned} \tag{3.58}$$

the equation becomes

$$\frac{\partial\hat{\Omega}}{\partial t} = \hat{\Omega}\left(2 - k_1^2 e^{2(1+\lambda)t} - k_2^2 e^{2(1-\lambda)t}\right) + \frac{2}{\pi}k_2 e^{2(1-\lambda)t}\tilde{\Omega}(k_1, 0, t). \tag{3.59}$$

Writing this in terms of a derivative prefactor , $F(k1, k2, t)$,

$$\frac{d}{dt}\left[F(k1, k2, t)\hat{\Omega}(k_1, k_2, t)\right] = \frac{2}{\pi}k_2 e^{2(1-\lambda)t}F(k1, k2, t)\tilde{\Omega}(k_1, 0, t), \tag{3.60}$$

$$F(k1, k2, t) = e^{-2t}G_1(\lambda, t)\, G_2(\lambda, t), \tag{3.61}$$

$$G_n(\lambda, t) = \exp\left[\frac{k_n^2 e^{2(1-(-1)^n\lambda)t}}{2\left(1-(-1)^n\lambda\right)}\right]. \tag{3.62}$$

Upon integrating over time and solving for $\hat{\Omega}(k_1, k_2, t)$, we find

$$\begin{aligned} \hat{\Omega}(k_1, k_2, t) &= \hat{\Omega}(k_1, k_2, 0)\exp[2t]\frac{G_1(\lambda, 0)}{G_1(\lambda, t)}\frac{G_2(\lambda, 0)}{G_2(\lambda, t)} \\ &\quad + \frac{2}{\pi}k_2\int_0^t \tilde{\Omega}(k_1, 0, \tau)\exp[2t - 2\lambda\tau]\frac{G_1(\lambda, \tau)}{G_1(\lambda, t)}\frac{G_2(\lambda, \tau)}{G_2(\lambda, t)}d\tau. \end{aligned} \tag{3.63}$$

Transforming the vorticity back into physical space yields

$$\begin{aligned} \Omega(X, Y, t) &= e^{2t}\int_{-\infty}^\infty\int_0^\infty \hat{\Omega}(k_1, k_2, 0)\frac{G_1(\lambda, 0)}{G_1(\lambda, t)}\frac{G_2(\lambda, 0)}{G_2(\lambda, t)}e^{-ik_1 X}\sin(k_2 Y)\, dk_1 dk_2 \\ &\quad + \sqrt{\frac{2}{\pi}}\int_0^t e^{2t-2\lambda\tau}\frac{(\lambda-1)^{\frac{3}{2}}\, Y\exp\left[\frac{(1-\lambda)Y^2/2}{e^{2(1-\lambda)\tau}-e^{2(1-\lambda)t}}\right]}{\left(e^{2(1-\lambda)t}-e^{2(1-\lambda)\tau}\right)^{\frac{3}{2}}} \\ &\quad \cdot\int_{-\infty}^\infty \tilde{\Omega}(k_1, 0, \tau)\frac{G_1(\lambda, \tau)}{G_1(\lambda, t)}e^{-ik_1 X}dk_1 d\tau. \end{aligned} \tag{3.64}$$

Thus, given an initial distribution and boundary condition defined by

$$\begin{aligned} &\omega(Xe^{-(1+\lambda)t}, 0, t) = \Omega(X, 0, t), \quad -\infty < x < \infty, \\ &\omega(x, y, 0) = \Omega(X, Y, 0), \qquad\qquad 0 < y < \infty, \end{aligned} \tag{3.65}$$

we can determine the nature of the tail. First we assume that the effect of vorticity is negligible in this region and set the initial distribution of vorticity, $\omega(x, y, 0)$, equal to zero. As an approximation, we assume that the vorticity introduced at the boundary of this region is in the form of a delta function of magnitude A, so that $\omega(x, y = 0, t) = A\delta(x)$. With these simplifications, the vorticity becomes,

$$\omega(x, y, t) = Ay\sqrt{\frac{1}{\pi}}\int_0^1 \frac{t \exp\left[-(1-\lambda)t\tau - \frac{x^2/2}{P(\tau)} - \frac{y^2/2}{Q(\tau)}\right]}{\sqrt{-P(\tau)\,Q(\tau)^3}} d\tau, \tag{3.66}$$

where

$$\begin{aligned} P(\tau) &= \frac{1 - e^{-2(1+\lambda)t\tau}}{1+\lambda}, \\ Q(\tau) &= \frac{1 - e^{-2(1-\lambda)t\tau}}{1-\lambda}. \end{aligned} \tag{3.67}$$

This shows that, as $t \to \infty$, far enough away from the stagnation point, so that the delta function approximation becomes a second order correction, the vorticity takes the form,

$$\omega(x, y, t) = \sqrt{\frac{1}{\pi}}\sqrt{\frac{\lambda+1}{\lambda-1}}\frac{A}{y}e^{-(1+\lambda)x^2/2} + O(\frac{1}{t}), \tag{3.68}$$

which is an approximation to the tail of vorticity in question. This tail has a Gaussian cross section with width $\sqrt{2/(1+\lambda)}$, which is equivalent to the width of a vortex sheet (2.5) embedded in the same strain field. Comparing this model to numerical results from a time advancing code, not shown presently, indicated that this estimate of the width of the tail is very good. Table 3.2 and Figure 3.12 show that, at $R = 100$, $\lambda = 1.5$, the tail has a width close to $\sqrt{2/(1+\lambda)} = 0.8$.

To find the rate of circulation increase, the vorticity distribution (3.66) may be

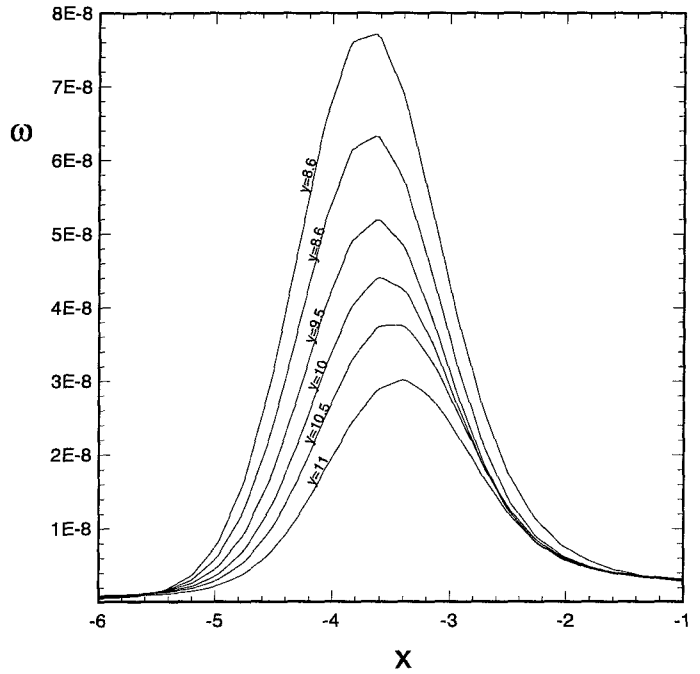

Figure 3.12: Cross-sections of "tail" at various y at $R = 100$, $\lambda = 1.5$.

integrated directly to give

$$\frac{\partial \Gamma}{\partial t} = \frac{\partial}{\partial t}\int_{-\infty}^{\infty}\int_{0}^{\infty} \omega(x,y,t)dxdy = \sqrt{\frac{2\left(\lambda-1\right)}{\pi}}\frac{A}{\sqrt{1-e^{2(1-\lambda)t}}}, \tag{3.69}$$

which, as $t \longrightarrow \infty$, limits to,

$$\frac{\partial \Gamma}{\partial t} = \sqrt{\frac{2\left(\lambda-1\right)}{\pi}}A. \tag{3.70}$$

Matching this circulation increase to (3.51) requires that

$$A = \frac{.48475\gamma}{8\varepsilon\sqrt{2\pi\left(\lambda-1\right)}}\Gamma \exp\left(\frac{-1}{2e\varepsilon}\right). \tag{3.71}$$

This value is physically reasonable because it shows that the delta function will be proportional to the cat's-eye boundary vorticity, $\sim \Gamma\gamma \exp(1/2e\varepsilon)$ and the length of the cat's-eye, $\sim \varepsilon^{-1/2}$, for large strain ratio, $\lambda = O\left(\varepsilon^{-1}\right)$.

These results indicate that the vorticity convected out of the cat's-eye develops into a tail of vorticity emanating from the stagnation points achieving a characteristic width equal to that of the Burgers vortex layer. The ability to match vorticity leakage

Table 3.2: Results of curve-fitting a Gaussian, $\omega e^{-(x-x_0)^2/\sigma^2}$, to the tail cross section at $R = 100$, $\lambda = 1.5$. Our analysis predicts $\sigma^2 = 0.8$.

x_0	y	ω	σ^2
3.70	8.6	7.8E-8	0.77
3.67	9.0	6.4E-8	0.75
3.63	9.5	5.2E-8	0.77
3.57	10.0	4.4E-8	0.79
3.50	10.5	3.8E-8	0.79
3.43	11.0	3.0E-8	0.79

from one region to the other gives us confidence that our various approximations are physically valid.

Chapter 4 Two-Dimensional Stability of the Axisymmetric Burgers Vortex

In this section we study the stability of the axisymmetric Burgers vortex to infinitesimal two-dimensional perturbations. These are defined as disturbances for which the velocity perturbations are in the $(x\text{-}y)$ plane normal to the axis of the vortex. The stability of the nonsymmetric case is considered in Chapter 5.

4.1 Basic equations

The problem will be formulated in the cylindrical polar coordinate system (r, θ, z) where the velocity field in the respective directions will be denoted by $\vec{u} = (u_r, u_\theta, u_z)$. This velocity field is decomposed as

$$u_r = -\frac{\gamma}{2} r + \hat{u}_r(r, \theta, t), \tag{4.1}$$

$$u_\theta = \hat{u}_\theta(r, \theta, t), \tag{4.2}$$

$$u_z = \gamma z, \tag{4.3}$$

where $\hat{u}_r$ and $\hat{u}_\theta$ are the rotational part of the velocity field and γ is the rate of strain in the z-direction corresponding to a uniform axisymmetric external strain. Substitution of (4.1)-(4.3) into the vorticity equation gives

$$\frac{\partial \omega}{\partial t} + u_r \frac{\partial \omega}{\partial r} + \frac{u_\theta}{r} \frac{\partial \omega}{\partial \theta} = \gamma \omega + \frac{\nu}{r} \left[\frac{\partial}{\partial r} \left(r \frac{\partial \omega}{\partial r} \right) + \frac{1}{r} \frac{\partial^2 \omega}{\partial \theta^2} \right], \tag{4.4}$$

where the vorticity field is non-zero only in the z-direction $\vec{\omega} = (0, 0, \omega)$.

4.2 2-D linearized stability analysis

4.2.1 Formulation

While the stability of (1.3)–(1.4) to three-dimensional perturbations is of fundamental interest, we presently consider the stability to two-dimensional disturbances. All quantities are non-dimensionalized with respect to length scale $\sqrt{\nu/\gamma}$ and time scale γ^{-1}. The two-dimensional perturbed velocity field in the r–θ plane is

$$\begin{aligned} u_r &= u_{r0} + u_r'(r,\theta,t), \\ u_\theta &= u_{\theta 0} + u_\theta'(r,\theta,t), \\ \omega &= \omega_0 + \omega'(r,\theta,t). \end{aligned} \tag{4.5}$$

A perturbation streamfunction ψ' can be defined such that

$$u_r' = \frac{1}{r}\frac{\partial \psi'}{\partial \theta}, \qquad u_\theta' = -\frac{\partial \psi'}{\partial r}, \tag{4.6}$$

$$\nabla^2 \psi' = -\omega'. \tag{4.7}$$

The perturbations are assumed to be of the normal mode form

$$\omega' = \omega(r) e^{-\mu t + in\theta}, \tag{4.8}$$

$$\psi' = \psi(r) e^{-\mu t + in\theta}, \tag{4.9}$$

where n is the azimuthal mode and $-\mu$ is the complex growth rate of the perturbation. In this formulation, unstable solutions correspond to negative values of the real part of μ. Using (4.6)–(4.9) in (4.4) and linearizing, it is found that

$$L^n \omega + \mu \omega = inR\left[-f\psi + \tfrac{1}{2} g\omega\right], \tag{4.10}$$

$$M^n \psi = -\omega, \tag{4.11}$$

where $R = \Gamma/2\pi\nu$ is a Reynolds number, the primes on the perturbation variables have been dropped for convenience, and

$$M^n(\cdot) \equiv \frac{1}{r}\frac{d}{dr}\left(r\frac{d}{dr}(\cdot)\right) - \frac{n^2}{r^2}(\cdot), \tag{4.12}$$

$$L^n(\cdot) \equiv M^n(\cdot) + \frac{1}{r}\frac{d}{dr}\left[r^2(\cdot)\right], \tag{4.13}$$

$$f \equiv e^{-r^2/2}, \quad g \equiv \frac{1-e^{-r^2/2}}{(r^2/2)}. \tag{4.14}$$

The first part of the RS84 analysis dealt with the special case of $R = 0$, the Stokes limit of (1)–(4) with the present scaling. Solutions were found in terms of the confluent hypergeometric function and, enforcing exponential decay at infinity, gave eigenvalues $\mu = n + 2k$, $k = 0, 1, 2, \ldots$. Since the eigenvalues are all positive real, the Burgers vortex is stable for zero circulation. The $R = 0$ normalized vorticity eigenfunctions are

$$\omega(n,k) = 2^{-n/2} r^n e^{-r^2/2} L_k^{(n)}\left(r^2/2\right), \tag{4.15}$$

where $L_k^n(x)$ is the generalized Laguerre polynomial. The streamfunction eigenfunctions can be found by integrating the vorticity eigenfunctions to give

$$\psi(r;n,0) = \frac{1}{2}\frac{\Gamma(n)}{(r^2/2)^{n/2}}\left[1 - e_{n-1}(r^2/2)e^{-r^2/2}\right], \tag{4.16}$$

$$\psi(r;n,k) = \frac{1}{2k} r^n e^{-r^2/2} L_{k-1}^{(n)}\left(r^2/2\right), \tag{4.17}$$

where e_{n-1} is the exponential series truncated after $n-1$ terms.

4.2.2 Numerical analysis using spectral methods

In order to tackle the problem numerically, we first obtain from (4.10)–(4.11) one equation for the vorticity,

$$\mathcal{L}(\omega) = -\mu\omega, \tag{4.18}$$

which is a complex eigenvalue problem with

$$\mathcal{L}(\cdot) = L^n(\cdot) - inR\left[f(M^n)^{-1}(\cdot) + \frac{1}{2}g(\cdot)\right]. \tag{4.19}$$

The behavior at the boundaries for the finite Reynolds number problem is identical to that found for the $R = 0$ case. Using boundedness of solutions and a Frobenius method about the regular singular point, $r = 0$, we find the behavior of the vorticity to be

$$\omega = O(r^n), \quad r \to 0. \tag{4.20}$$

For $r \to \infty$, a dominant balance argument is used to write equation (4.18) as

$$\frac{1}{r}\frac{d}{dr}\left(r\frac{d}{dr}\omega\right) - \frac{n^2}{r^2}\omega + \frac{1}{r}\frac{d}{dr}\left[r^2\omega\right] + \mu\omega = \frac{inR\omega}{r^2}, \tag{4.21}$$

which can be written simply as

$$L^{(n^2+inR)^{1/2}}(\omega) + \mu\omega = 0, \tag{4.22}$$

so that the behavior at infinity remains the same as for $R = 0$,

$$\omega \sim Ar^{\mu}e^{-r^2/2}, \quad r \to \infty. \tag{4.23}$$

Since the RS analysis for $R = 0$ resulted in a set of eigenfunctions that spanned the space with the specified boundary conditions, it is natural to use spectral methods for numerical purposes. A Galerkin approach is used to expand solutions in the orthogonal basis defined by the $R = 0$ vorticity eigenfunctions

$$\omega = \sum_{k=0}^{N-1} a_k\, \omega(r; n, k), \quad \omega(r; n, k) = 2^{-n/2}r^n e^{-r^2/2}L_k^{(n)}\left(r^2/2\right), \tag{4.24}$$

where the finite expansion is truncated at $N - 1$ terms. Substitution of (4.24) into

(4.18) results in a complex eigenvalue problem of the form

$$\mathbf{A}\vec{x} = -\mu\vec{x}, \tag{4.25}$$

where $\vec{x} = (a_0, a_1, ..., a_{N-1})^T$ and $\mathbf{A}$ is complex matrix of order $N \times N$ whose coefficients are found by using the orthogonality of the basis functions under the weighted inner product,

$$\langle u, v\rangle = \int_0^\infty u\bar{v}e^{r^2/2}rdr, \tag{4.26}$$

such that the coefficients of $\mathbf{A}$,

$$\mathbf{A}_{jk} = \frac{\left\langle \omega_j^n(r), \mathcal{L}\omega_k^n(r)\right\rangle}{\left\langle \omega_j^n(r), \omega_j^n(r)\right\rangle}, \tag{4.27}$$

follow from

$$\left\langle \omega_j^n(r), \omega_k^n(r)\right\rangle = \begin{cases} 0 & \text{if } k \neq j, \\ \frac{(n+j)!}{j!} & \text{if } k = j, \end{cases}, \tag{4.28}$$

$$\left\langle \omega_j^n(r), L^n\omega_k^n(r)\right\rangle = \begin{cases} 0 & \text{if } k \neq j, \\ (n+2j)\frac{(n+j)!}{j!} & \text{if } k = j, \end{cases}, \tag{4.29}$$

$$\left\langle \omega_j^n(r), f(M^n)^{-1}\omega_k^n(r)\right\rangle = -2^{-(n+j+k+1)}\frac{(j+k+n-1)!}{j!\ k!}, \tag{4.30}$$

$$\left\langle \omega_j^n(r), g\omega_k^n(r)\right\rangle = \frac{(n+\min(k,l))!}{n\ \min(k,l)!} - \sum_{q=0}^{j}\sum_{p=0}^{k} 2^{-(p+q+n)}\frac{(p+q+n-1)!}{p!\ q!}. \tag{4.31}$$

4.3 Results

By construction, this method reproduces the known eigensolutions for $R = 0$. Results for larger Reynolds number are plotted in Figures 4.1–4.4 for the values of the parameter $n = 1, 2, 3$ and 4, respectively. Numerical solutions to (4.25) are found using the QZ algorithm for values of N ranging from 20 to 300. For fixed N and n, we find a denumerable set of eigenfunctions and eigenvalues for $k = 0, 1, 2, ...$, each

corresponding to a different radial structure of the perturbation. These calculations are tested in various ways. First, for low Reynolds number, our results are compared to RS84 results and are found to agree well (see Table 4.1 and subsequent discussion). Next, for fixed R, the dimension N is increased until convergence is evident. Thirdly, results for Reynolds numbers up to approximately 100 are checked by treating the problem as a nonlinear continuation in the parameter R, starting at $R = 0$, using a Newton-Raphson scheme with finite-difference techniques.

RS did analyze the effect of non-zero Reynolds number by way of a perturbation expansion for small R and found that for the eigenvalue expansion

$$\mu = \mu_0 + \mu_1 R + \mu_2 R^2 + \cdots, \tag{4.32}$$

$\mu_0 = n + 2k$ and the coefficients μ_1 and μ_2 were given by RS:{(2.15)–(2.19)}. Since μ_1 is strictly imaginary its value does not affect the stability of the vortex. For low values of k, μ_2 is positive and thereby serves only to increase the value of $\mathrm{Re}(\mu)$. We have calculated μ_1 and μ_2 to larger k than RS, and find that, for fixed n, μ_2 can become negative at sufficiently large k (see Table 4.1). This is equivalent to $(\partial^2\mu/\partial R^2)_{R=0} < 0$ and indicates a trend towards possible instability at values of R beyond the validity of (4.32).

Values of $n = 1, ..., 10$ are calculated. In all cases, as illustrated in Figures 4.1–4.4, the $\mathrm{Re}(\mu) > 0$, indicating stability of the Burgers vortex to two-dimensional perturbations. Note that for values of (n, k), where (4.32) indicates $(\partial^2\mu/\partial R^2)_{R=0} < 0$, we find that $\mathrm{Re}(\mu)$ reaches a local minimum followed by a subsequent increase with increasing R. This behavior is on a scale too small to be seen graphically in Figures 4.1–4.4. Numerical results at high Reynolds indicate that the real part of the of the eigenvalue grows like the square root of the Reynolds number. The irregularity of the plots at large Reynolds number is caused by resolution problems in representing the vorticity with a maximum number of basis functions, $N = 300$.

The graphs of the real part of the eigenfunction shown in Figures 4.5–4.6 indicate that as the Reynolds number increases, the eigenfunction maximum moves outward

in radius. Moreover, the function becomes more and more oscillatory, but confined to within a narrow radial band. It is this structure that limits the range of our finite-difference method to maximum $R \sim 10^2$ and that of the spectral method to maximum $R \sim 10^4$.

4.3.1 Summary

The stability of the axisymmetric Burgers vortex solution of the Navier-Stokes equations to two-dimensional perturbations is studied numerically up to Reynolds numbers of order 10^4. We find no unstable eigenmodes for azimuthal mode numbers $n = 1, \ldots 10$ in this range of Reynolds numbers. Increasing the Reynolds number has a stabilizing effect on the vortex.

Table 4.1: Comparison with Robinson and Saffman's results for Small Reynolds number, $N = 50$, $\mu = \mu_0 + R\mu_1 + R^2\mu_2$

n	k	$-i\mu_1$ (RS)	$-i\mu_1$	$10^2\mu_2$ (RS)	$10^2\mu_2$
1	0	0 .	0.00000000	0.	0.00000000
1	1	0.125	0.12499977	0.14435071	0.14435055
1	2	0.125	0.12500003	0.10094794	0.10094833
⋮	⋮	⋮	⋮	⋮	⋮
1	7	0.0916443	0.09164255	0.00225961	0.00225988
1	8	0.0872803	0.08728127	-0.000431672	-0.00043345
1	9	0.0834618	0.08346671	-0.00207814	-0.00207772
2	0	0.025	0.02499994	0.27855829	0.27855588
2	1	0.025	0.02499994	0.42798057	0.42798354
2	2	0.0234375	0.02343752	0.02636197	0.02636217
⋮	⋮	⋮	⋮	⋮	⋮
2	8	0.166924	0.16692388	0.00340799	0.00340921
2	9	0.160179	0.16017876	-0.00284228	-0.00284910
2	10	0.154172	0.15417211	-0.00697667	-0.00697291
3	0	0.0375	0.03749983	0.85088957	0.85088854
3	1	0.034375	0.03437489	0.64678972	0.64679239
3	2	0.03203125	0.03203126	0.43069801	0.43070205
⋮	⋮	⋮	⋮	⋮	⋮
3	10	0.220477	0.22048121	0.00131356	0.00131323
3	11	0.213431	0.21342685	-0.00600394	-0.00601022
3	12	0.20701	0.20722134	-0.0112759	-0.01131203

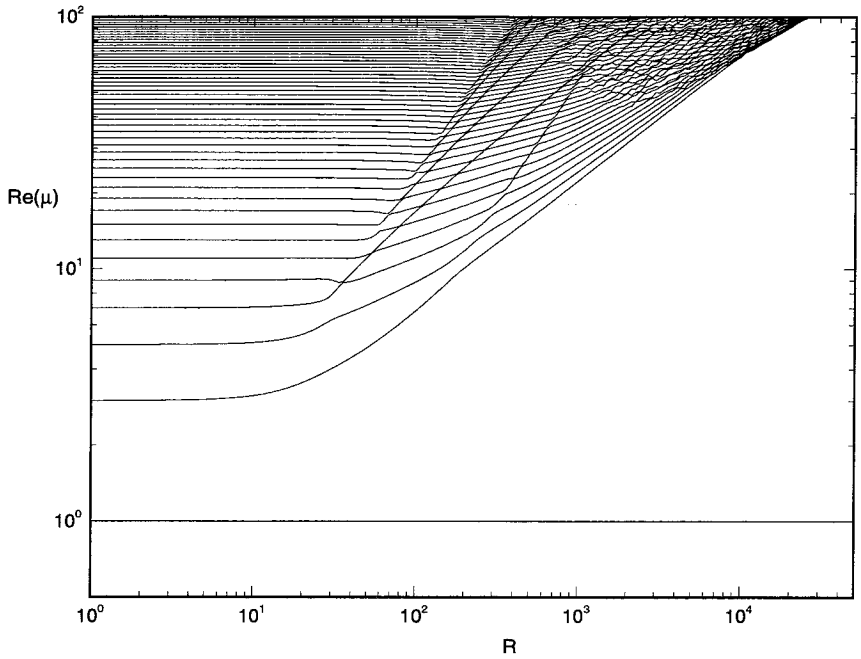

Figure 4.1: Real part of the eigenvalues vs. Reynolds number for $n = 1, N = 300, k = 0, 1, 2, ...$ defined by the y-axis intercept, $n + 2k$.

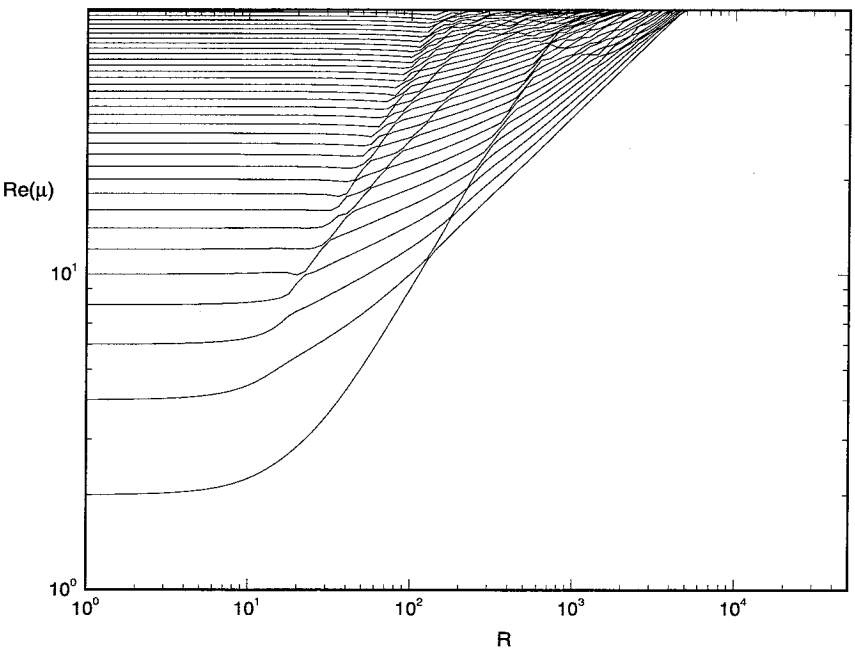

Figure 4.2: Real part of the eigenvalues vs. Reynolds number for $n = 2, N = 150, k = 0, 1, 2, ...$ defined by the y-axis intercept, $n + 2k$.

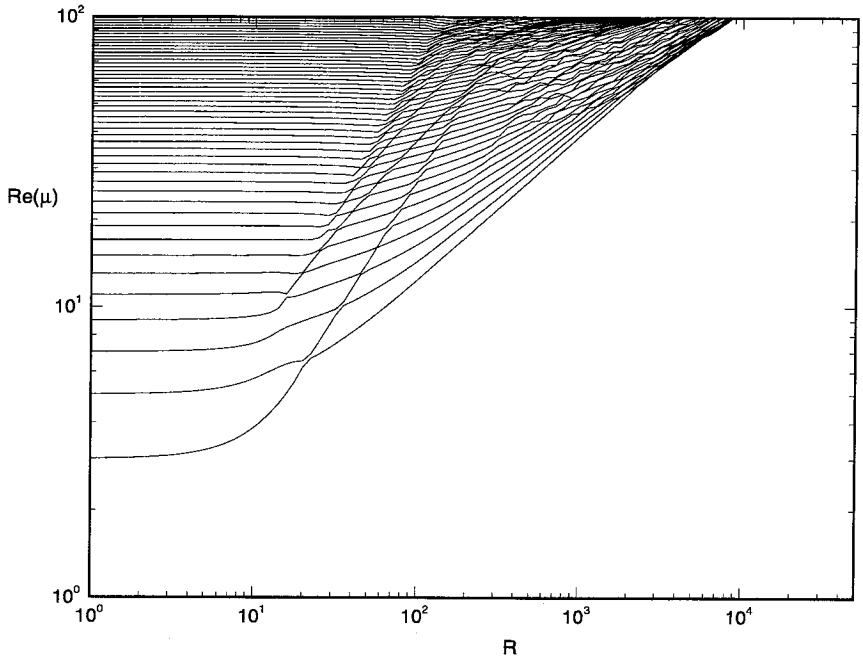

Figure 4.3: Real part of the eigenvalues vs. Reynolds number for $n = 3, N = 150, k = 0, 1, 2, ...$ defined by the y-axis intercept, $n + 2k$.

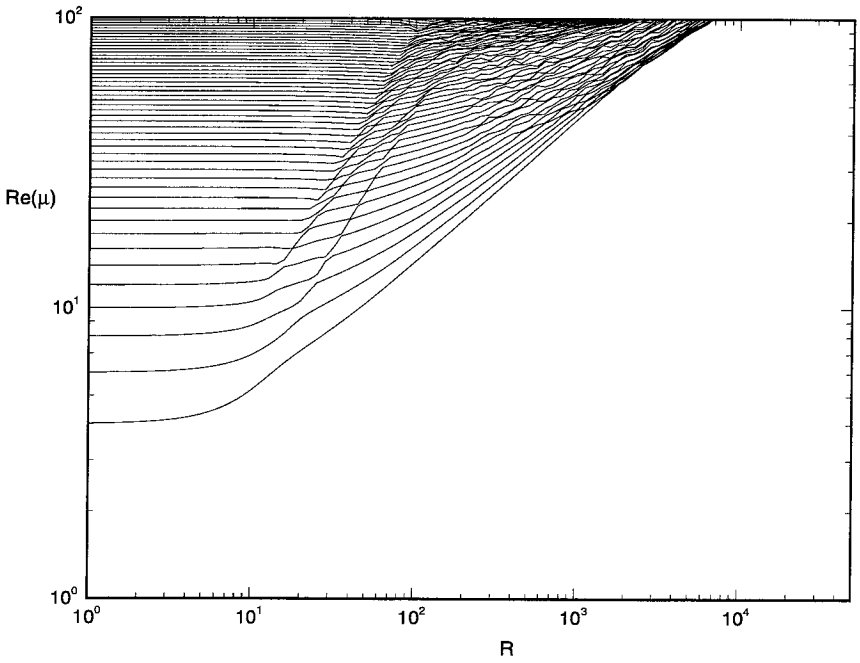

Figure 4.4: Real part of the eigenvalues vs. Reynolds number for $n = 4, N = 150, k = 0, 1, 2, ...$ defined by the y-axis intercept, $n + 2k$.

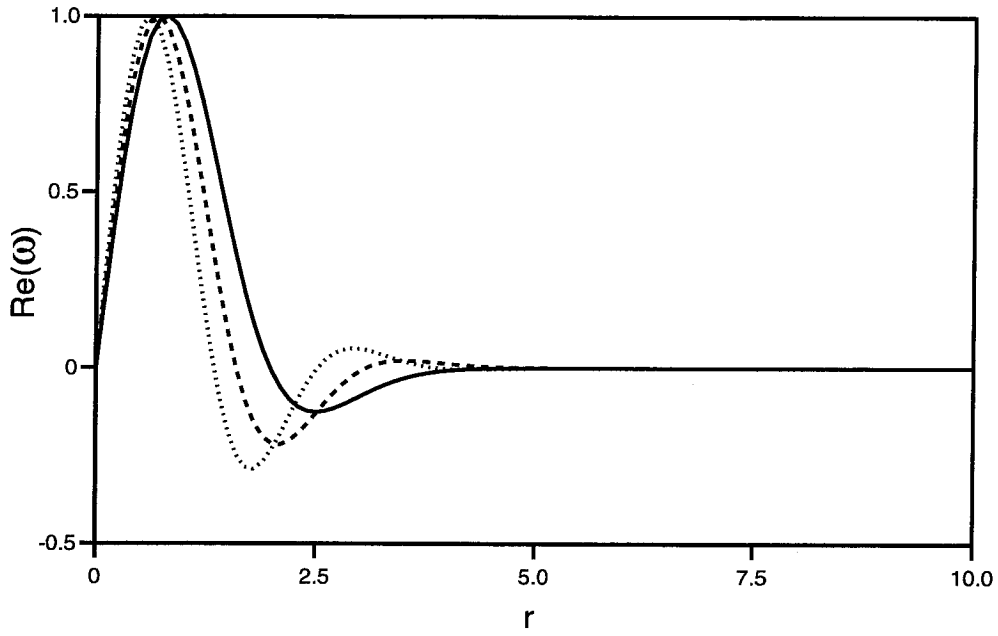

Figure 4.5: Real part of the eigenfunctions vs. radius for $n = 1, N = 300, R = 1.0, k = 1$(solid), 2(dashed), 3(dotted).

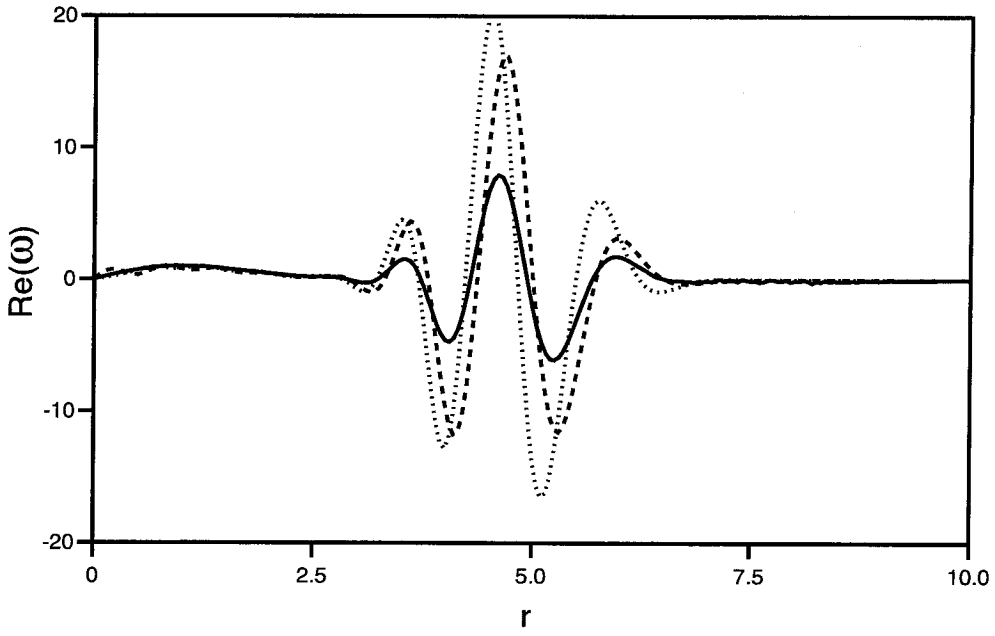

Figure 4.6: Real part of the eigenfunctions vs. radius for $n = 1, N = 300, R = 1000, k = 1$(solid), 2(dashed), 3(dotted).

Chapter 5 Two-Dimensional Stability of Nonsymmetric Burgers Vortices

We now consider the linear stability of the steady solutions discussed in Chapter 2. We begin by demonstrating a property of general solutions of the vorticity equation for vorticity distributions in the presence of a linear background velocity field.

5.1 General vorticity in a linear velocity field

We return briefly to dimensional coordinates and consider a velocity field of the form

$$u_i = \bar{u}_i(x_i, t) + J_{ij}(t)\, x_j, \tag{5.1}$$

where (5.1) represents a general velocity field $\bar{u}$ embedded in a linear background field. We take Cartesian coordinates $x_i \equiv (x_1, x_2, x_3)$ aligned with the nonrotating principal rates of strain with $\alpha(t) + \beta(t) + \gamma(t) = 0$ and denote the background vorticity by ξ_i. The time-dependent rate-of-strain tensor of the background field is then

$$\mathbf{J}(t) = \mathbf{S}(t) + \mathbf{A}(t) = \begin{bmatrix} \alpha(t) & 0 & 0 \\ 0 & \beta(t) & 0 \\ 0 & 0 & \gamma(t) \end{bmatrix} + \begin{bmatrix} 0 & \frac{1}{2}\xi_3(t) & -\frac{1}{2}\xi_2(t) \\ -\frac{1}{2}\xi_3(t) & 0 & \frac{1}{2}\xi_1(t) \\ \frac{1}{2}\xi_2(t) & -\frac{1}{2}\xi_1(t) & 0 \end{bmatrix}. \tag{5.2}$$

The vorticity equation, then, in indicial notation is given by

$$\frac{\partial \omega_i}{\partial t} + J_{jk}x_k\frac{\partial \omega_i}{\partial x_j} + \bar{u}_j\frac{\partial \omega_i}{\partial x_j} = \omega_j\frac{\partial \bar{u}_i}{\partial x_j} + J_{ij}\omega_j + \nu\nabla^2\omega_i, \tag{5.3}$$

where $\omega_i = \overline{\omega}_i + \xi_i = \epsilon_{ijk}(\partial u_j/\partial x_k) + \xi_i$. Making the change of variables to a system centered on a particle initially located at x_{0_i} moving with the background flow

$$x_i = X_i - x_{p_i}(t, x_{0_i}), \tag{5.4}$$

where

$$\frac{dx_{p_i}}{dt} = J_{ij}x_{p_i} \text{ with } x_{p_i}(0) = x_{0_i}, \tag{5.5}$$

gives

$$\frac{\partial \omega_i}{\partial t} + J_{jk}(X_k - x_{p_k})\frac{\partial \omega_i}{\partial X_j} + \bar{u}_j\frac{\partial \omega_i}{\partial X_j} = \omega_j\frac{\partial \bar{u}_i}{\partial X_j} + J_{ij}\omega_j + \nu\nabla^2\omega_i. \tag{5.6}$$

Now, if we define, transformed vorticity and velocity fields denoted by capitalized variables,

$$\begin{aligned} \Omega_i(X_i, t) &= \omega_i(X_i - x_{p_i}, t), \\ U_i(X_i, t) &= \overline{u}_i(X_i - x_{p_i}, t), \end{aligned} \tag{5.7}$$

then we see that Ω solves the vorticity equation

$$\frac{\partial \Omega_i}{\partial t} + J_{jk}X_k\frac{\partial \Omega_i}{\partial X_j} + U_j\frac{\partial \Omega_i}{\partial X_j} = \Omega_j\frac{\partial U_i}{\partial X_j} + J_{ij}\Omega_j + \nu\nabla^2\Omega_i, \tag{5.8}$$

which is identical in form to (5.3). Note that the boundary conditions on this transformed equation may indeed be time dependent if the solution to (5.3) corresponds to velocities that do not decay to zero at infinity.

From the above we can conclude that for a given solution to (5.3), there exists an infinite family of additional solutions (indexed by x_{0_i}), each with the same form and evolution, corresponding to a displacement of the initial vorticity by x_{0_i} and subsequent convection with the background flow. Alternatively we may say that solutions to (5.3) are invariant to an arbitrary initial displacement of the embedded vorticity field. We shall refer to this as the *neutrally convective* property of vorticity embedded in a linear field, and note that these results are also valid for the Euler and advection-diffusion equations. Furthermore, for the case of compact vorticity, we

should note that the background vorticity ξ_i must satisfy

$$\frac{\partial \xi_i}{\partial t} = J_{ij}\xi_j = S_{ij}\xi_j, \tag{5.9}$$

yielding an alternative form for (5.3),

$$\frac{\partial \overline{\omega}_i}{\partial t} + J_{jk}x_k\frac{\partial \overline{\omega}_i}{\partial x_j} + \bar{u}_j\frac{\partial \overline{\omega}_i}{\partial x_j} = \overline{\omega}_j\frac{\partial \bar{u}_i}{\partial x_j} + J_{ij}\overline{\omega}_j + S_{ij}\xi_j + \nu\nabla^2\omega_i. \tag{5.10}$$

5.2 A convectively neutral mode

We now apply this result to our solutions of (5.3) corresponding to steady vorticity in the z-direction, where the background flow is a steady constant (in time) linear strain with no shear, $\xi \equiv 0$. Equations (5.4) and (5.7) become

$$x = X - x_0e^{\alpha t}, \qquad y = Y - y_0e^{\beta t}, \tag{5.11}$$

$$\begin{aligned} \Omega(X,Y,t) &= \omega(X - x_0e^{\alpha t}, Y - y_0e^{\beta t}), \\ U(X,Y,t) &= \overline{u}(X - x_0e^{\alpha t}, Y - y_0e^{\beta t}), \\ V(X,Y,t) &= \overline{v}(X - x_0e^{\alpha t}, Y - y_0e^{\beta t}), \end{aligned} \tag{5.12}$$

and we see that $\Omega(X,Y,t)$ is a convecting solution of (1.1) in the form

$$\frac{\partial \Omega}{\partial t} + (\alpha X + U)\frac{\partial \Omega}{\partial X} + (\beta Y + V)\frac{\partial \Omega}{\partial Y} = \gamma\Omega + \nu\nabla^2\Omega. \tag{5.13}$$

To relate this result to linear stability analysis, we write a general perturbed vorticity field in the form

$$\omega(x,y,t) = \omega_{ss}(x,y) + \omega_1(x,y)e^{-\mu t}, \tag{5.14}$$

where ω_{ss} is the steady base state and ω_1, $|\omega_1| \ll |\omega_{ss}|$, and μ are the eigenfunction and eigenvalue, respectively. Positive μ denotes linear stability and $\mu = 0$ is the neutral stability boundary. Next we apply the neutrally convective property to $\omega_{ss}(x,y)$

and Taylor expand to obtain,

$$\omega_{ss}(x - x_0 e^{\alpha t}, y - y_0 e^{\beta t}) \simeq \omega_{ss}(x, y) - \frac{\partial \omega}{\partial x} x_0 e^{\alpha t} - \frac{\partial \omega}{\partial y} y_0 e^{\beta t}. \tag{5.15}$$

Comparing the right-hand sides of (5.14)-(5.15) gives two linear eigensolutions $-\frac{\partial \omega}{\partial X} e^{\alpha t}$ and $-\frac{\partial \omega}{\partial Y} e^{\beta t}$ with corresponding eigenvalues $-\alpha$ and $-\beta$.

This result can be applied to various well known solutions of the Navier-Stokes equations. For the Burgers vortex, the axisymmetric strain rates are $\alpha = \beta = -\gamma/2$, so that, for any Reynolds number, this convective mode gives eigenvalue equal to $\gamma/2$. Given our nondimensionalization in Chapter 4, this explains the appearance of stable eigenvalue $\mu = 1$ for all Reynolds numbers in Figure 4.1. Secondly, for the Burgers vortex sheet solution (1.5) in plane strain, $\alpha = -\gamma, \beta = 0$, we see that a perturbation in the y-direction is neutrally stable, $\mu = 0$, but a displacement in x, results in a relaxation back to the base state. For the current study of nonsymmetric Burgers vortices, upon nondimensionalization and in terms of the strain ratio, the strain rates of the nonsymmetric strain field result in eigenvalues of $\mu_1 = 1 + \lambda$ and $\mu_2 = 1 - \lambda$. Thus for $\lambda > 1$, there exists at least one positive eigenvalue and therefore a linearly unstable mode. This does not correspond to a structural instability of the steady nonsymmetric vortex but is merely the early-time linear phase of the non-linear neutrally convective mode discussed previously.

5.3 Subspace iteration

In order to determine the stability boundary of the nonsymmetric Burgers vortex in the R-λ plane, we use a time advancing code in conjunction with a subspace iteration method to capture the fastest growing modes of the perturbation (Saad [18]). We restrict attention to two-dimensional perturbations, that is, those with velocity components normal to the steady vorticity. We now return to nondimensional coordinates and write (2.1) in terms of nondimensional cylindrical polar coordinate

system, (r, θ, z),

$$\begin{aligned}\frac{\partial \omega}{\partial t} &= \frac{1}{r}\left[\frac{\partial}{\partial r}\left(r\frac{\partial \omega}{\partial r}\right) + \frac{1}{r}\frac{\partial^2 \omega}{\partial \theta^2}\right] + \left[r(\lambda \cos 2\theta - 1) - Ru_r\right] \\ &\quad + \left[\lambda \sin 2\theta - \frac{Ru_\theta}{r}\right]\frac{\partial \omega}{\partial \theta} + 2\omega \end{aligned} \tag{5.16}$$

$$\nabla^2 \psi = -\omega, \quad u_r = \frac{1}{r}\frac{\partial \psi}{\partial \theta}, \quad u_\theta = -\frac{\partial \psi}{\partial r}, \tag{5.17}$$

where the velocity induced by the vorticity is now $\mathbf{u} = (u_r, u_\theta, 0)$. We linearize the equations with

$$\begin{aligned}\omega &= \omega + \omega', \\ u_r &= u_{r_0} + u_r', \\ u_\theta &= u_{\theta_0} + u_\theta', \end{aligned} \tag{5.18}$$

where primed quantities are small perturbations, and we solve the resulting linear set using finite-difference methods in r and spectral methods in θ (Buntine and Pullin [3]). Taking the discrete Fourier transforms,

$$\omega'(r, \theta, t) = e^{-\mu t} \sum_{n=-\frac{1}{2}N}^{\frac{1}{2}N-1} \hat{\omega}_n(r) e^{in\theta}, \tag{5.19}$$

$$\psi'(r, \theta, t) = e^{-\mu t} \sum_{n=-\frac{1}{2}N}^{\frac{1}{2}N-1} \hat{\psi}_n(r) e^{in\theta}, \tag{5.20}$$

the Poisson equation becomes,

$$\frac{d^2 \hat{\psi}_n}{dr^2} + \frac{1}{r}\frac{d\hat{\psi}_n}{dr} - \frac{n^2}{r^2}\psi_n = -\hat{\omega}_n \tag{5.21}$$

and the linearized vorticity equation becomes,

$$\frac{\partial \hat{\omega}_n}{\partial t} = \frac{-\lambda}{r}\left[\frac{\partial}{\partial r}\left(r^2 \hat{\omega}_{n+2}\right) + \frac{\partial}{\partial r}\left(r^2 \hat{\omega}_{n-2}\right)\right] - \lambda\left[(n+2)\,\hat{\omega}_{n+2} - (n-2)\,\hat{\omega}_{n-2}\right]$$

$$+\frac{1}{r}\frac{\partial}{\partial r}\left(r^2\hat{\omega}_n\right)+\left[\frac{\partial^2\hat{\omega}_n}{\partial r^2}+\frac{1}{r}\frac{\partial\hat{\omega}_n}{\partial r}-\frac{n^2}{r^2}\hat{\omega}_n\right] \tag{5.22}$$
$$-\left[u_{r_0}\frac{\partial\omega'}{\partial r}+\frac{1}{r}u_{\theta_0}\frac{\partial\omega}{\partial\theta}+u'_r\frac{\partial\omega_0}{\partial r}+\frac{1}{r}u'_\theta\frac{\partial\omega_0}{\partial\theta}\right],$$

for $N=-N/2,\ldots,N/2-1$. The boundary conditions on $(5.21-5.22)$ are

$$r=0: \quad \hat{\psi}_n=0, \tag{5.23}$$
$$\hat{\omega}_n=0, n\neq 0,$$
$$\frac{d\hat{\omega}_0}{dr}=0,$$
$$r\to\infty: \quad \hat{\psi}_n(r)\to 0, \tag{5.24}$$
$$\hat{\omega}_n(r)\to 0.$$

Equation (5.22) is solved by a fourth-order five point spatial finite difference scheme. The system is advanced in time first with a second-order explicit predictor followed by updating the vorticity in a Crank Nicolson, semi-implicit, two-point corrector scheme. This updated vorticity $\hat{\omega}(t+\delta t)$ is then used in the Poisson solver. Several iterations of this procedure are needed per time step for convergence. Further details of the scheme are given in Buntine and Pullin [3]. All calculations reported presently use $N=256$ in (5.19)–(5.20). Initial conditions are obtained from the steady solutions of Chapter 2 by projection of the steady values of ω and ψ onto the r-θ grid.

Initially, a simple power method approach is used in which, if we represent the time advancement as the function A, a random initial guess, $\hat{\omega}$, is iterated on A, *i.e.*,

$$\hat{\omega}_{k+1}=\frac{1}{|\hat{\omega}_{k+1}|}A\hat{\omega}_k, \tag{5.25}$$

where k denotes the iteration number and $|\hat{\omega}_{k+1}|$ is the L^2 norm of the vector $A\hat{\omega}_k$. The eigenvalue is then calculated using the Rayleigh quotient,

$$\mu_k=\frac{\langle A\omega_k,\omega_k\rangle}{\langle\omega_k,\omega_k\rangle}. \tag{5.26}$$

Iteration is continued until $|\mu_k - \mu_{k-1}| < 10^{-3}$. Maximum eigenvalues are found using this method for $R = 1, 10, 100$, and 1000 and are shown in Tables 5.1–5.2. From these results it is seen that the eigenvalue corresponding to the fastest growing eigenfunction corresponds closely to $\mu = 1 - \lambda$. The corresponding numerically-obtained eigenfunctions are also found to be closely proportional to $\partial\omega_{ss}/\partial y$. We may thus conclude that mode with maximum growth rate corresponds to a neutrally convective translation of the nonsymmetric vortex without change of shape and that this convection is toward the origin for $\lambda < 1$. Therefore, all eigenvalues are positive for $\lambda < 1$ and the nonsymmetric Burgers vortex is linearly stable in this region, at least for the values of R investigated.

In the region $\lambda > 1$, these eigenvalues are positive, allowing the possibility that other eigenfunctions exist with $0 < \mu < 1-\lambda$ that are not convectively neutral. These eigenfunctions are examined by employing a multi-step subspace iteration technique (Saad [18]) in which we iterate on the three vector system $W_k = (\hat{\omega}_1, \hat{\omega}_2, \hat{\omega}_3)$, where $\hat{\omega}_1$ and $\hat{\omega}_2$ are equal to the analytical form of the convectively neutral eigenfunctions and $\hat{\omega}_3$ is a random vector. We calculate

$$V_{k+1} = A^p W_k \tag{5.27}$$

and compute the QR factorization $V_{k+1} = QR$ to find $W_{k+1} = Q$. Since the cost of this orthonormalization can be high, it is only performed after p iterations on A. Computing the Rayleigh quotients yield the two analytically predicted eigenvalues $1 \pm \lambda$ and a third eigenvalue which corresponds to the fastest growing eigenfunction not found previously. This eigenfunction consistently corresponds to an eigenvalue approximately equal to 0 within our numerical accuracy for all Reynolds numbers studied. We hypothesize that this eigenmode represents the exceedingly slow evolution of the quasi-steady numerical solutions for nonsymmetric Burgers vortices with $\lambda > 1$. We subsequently argue that this comprises leakage of vorticity occurring near stagnation points of the steady flow. A model for this leakage was discussed in the Chapter 3.

5.4 Results

The linear stability analysis has analytically shown that at least one positive eigenvalue exists for $\lambda > 1$. Our result shows that in a biaxial strain field, a general, small perturbation to the vortex will result in the vortex moving with the strain field.

For the range of Reynolds numbers investigated, $R = 1, 10, 100, 1000$, we find that the two smallest (most negative) eigenvalues in fact do correspond to the translating analytical solutions found in the previous section for $\lambda < 1$. For $\lambda > 1$, the smallest eigenvalue, $1 - \lambda$, corresponds to the convectively neutral mode and the second smallest eigenvalue, ≈ 0, corresponds to the slow leakage of vorticity into tails.

Table 5.1: Maximum eigenvalue for $R = 1, 10$

λ	$\mu_{\max}, R = 1$	$\mu_{\max}, R = 10$
0.2	0.8168	0.8014
0.4	0.6093	0.6050
0.6	0.4040	0.4033
0.8	0.2058	0.2046

Table 5.2: Maximum eigenvalue for $R = 100, 1000$

λ	$\mu_{\max}, R = 100$	$\mu_{\max}, R = 1000$
0.5	0.5056	-
1.0	0.0203	0.0126
1.5	-0.5031	-
2.0	-	-0.9956
3.0	-	-1.9965

Chapter 6 Summary

6.1 Conclusions

The major results and conclusions are the following:

- The steady and quasi-steady structure of nonsymmetric Burgers vortices was calculated numerically for a wide range of strain ratios ($0.2 < \lambda < 150$) and Reynolds numbers ($1 < R < 10^4$), which includes strain ratios well into the biaxial region, $\lambda > 1$.

- An asymptotic formulation for the analytic form of the vorticity for large R and λ but $\varepsilon \ll 1$, in the region outside of the core of the vorticity but within the cat's-eye boundary was derived to be

$$\omega_{\text{II}}(r,\theta) = Re^{-\frac{r^2}{2}\exp(\varepsilon r^2 \sin 2\theta)} \tag{6.1}$$

  and found the associated velocities which were exponentially small in this region. Furthermore, this asymptotic formulation was generalized for a Burgers vortex embedded in a straining field composed of axismmetric and purely two-dimenensional strain.

- An estimate for the flux of vorticity out of the cat's-eye was made and the decay of circulation was found to be exponentially small,

$$\frac{\partial \Gamma}{\partial t} = \frac{.48475}{4\pi}\gamma\varepsilon^{-1}\Gamma \exp\left(\frac{-1}{2e\varepsilon}\right). \tag{6.2}$$

  and the structure of this leaking vorticity was found to be in the form of "tails" emanating from the stagnation points of the flow whose long time behavior closely resembled a time-dependent Burgers vortex layer.

- The axisymmetric Burgers vortex was shown to be linearly stable to two-dimensional perturbations for Reynolds number up to $10,000$.

- The nonsymmetric Burgers vortex was found to be linearly stable for $\lambda < 1$ and for $\lambda \geq 1$, the instability of the vortex corresponds to the vortex maintaining its structure while being convected with the background strain. An analytic explanation for this convectively neutral mode of instability which applies in general is presented.

Clearly, the structure and stability of Burgers-type vortices has been studied to great detail without the discovery of a stability boundary that could be applied to explaining the role of Burgers vortices in turbulence. The next step would appear to be consideration of the stability of the Burgers vortex to three-dimensional perturbations.

Appendix A Stability of Sullivan Vortices to 2-D Perturbations

A.1 Background

The Burgers vortex, while the most heavily studied stretched vortex, is only one of a class of solutions. R. D. Sullivan [6] introduced a solution to the Navier-Stokes equations, analogous to the Burgers' solution, in which the velocities were of the form

$$u_r = u_r(r), \tag{A.1}$$

$$u_\theta = u_\theta(r), \tag{A.2}$$

$$u_z = z u_z(r). \tag{A.3}$$

He in turn introduced a "two-cell" solution in which the flow does not only spiral in towards the z-axis and out along it, but instead has a region of reverse flow near the axis:

$$u_{r_0} = -\frac{\gamma}{2} r + \frac{6\nu}{r}\left[1 - e^{(-\gamma r^2/4\nu)}\right], \tag{A.4}$$

$$u_{\theta_0} = \frac{\Gamma}{2\pi r}\left[\frac{H(\gamma r^2/4\nu)}{H(\infty)}\right], \tag{A.5}$$

$$u_{z_0} = \gamma z\left[1 - 3e^{(-\gamma r^2/4\nu)}\right], \tag{A.6}$$

where,

$$H(x) = \int_0^x exp\left[-t + 3\int_0^t \left[(1 - e^{-\tau})/\tau\right] d\tau\right] dt. \tag{A.7}$$

We would like to determine if it is possible to construct a physically plausible two-dimensional linearized stability analysis similar to that in Chapter 4 where the velocities u_r, u_θ are perturbed and the perturbations can be written in streamfunction-

vorticity form.

Non-dimensionalizing time by $\gamma/2$ and length by $\sqrt{\gamma/2\nu}$, and using the Reynolds Number, $R = \Gamma/2\pi\nu$, we get

$$u_{r_0} = -r + \frac{6}{r}\left[1 - e^{(-r^2/2)}\right], \tag{A.8}$$

$$u_{\theta_0} = \frac{R}{r}\left[\frac{H(r^2/2)}{H(\infty)}\right], \tag{A.9}$$

$$u_{z_0} = 2z\left[1 - 3e^{(-r^2/2)}\right]. \tag{A.10}$$

Calculating the vorticity $\vec{\omega} = \vec{\nabla} \times \vec{u}$ of this velocity field yields

$$\omega_{r_0} = \frac{1}{r}\frac{\partial w}{\partial \theta} - \frac{\partial v}{\partial z} = 0, \tag{A.11}$$

$$\omega_{\theta_0} = \frac{\partial u}{\partial z} - \frac{\partial w}{\partial r} = -6rze^{(-r^2/2)}, \tag{A.12}$$

$$\omega_{z_0} = \frac{1}{r}\frac{\partial (rv)}{\partial r} - \frac{1}{r}\frac{\partial u}{\partial \theta} = R\frac{H'(r^2/2)}{H(\infty)}. \tag{A.13}$$

Assuming a form for the perturbations as in Chapter 4,

$$\begin{aligned} u_r &= u_{r_0} + u'_r(r,\theta,t), \\ u_\theta &= u_{\theta_0} + u'_\theta(r,\theta,t), \\ \omega &= \omega_{z_0} + \omega'(r,\theta,t), \end{aligned} \tag{A.14}$$

a perturbation streamfunction ψ' can be defined such that

$$u'_r = \frac{1}{r}\frac{\partial \psi'}{\partial \theta}, \qquad u'_\theta = -\frac{\partial \psi'}{\partial r}, \tag{A.15}$$

$$\nabla^2 \psi' = -\omega', \tag{A.16}$$

where the perturbations are assumed to be of the normal mode form

$$\omega' = \omega(r)e^{-\mu t + in\theta}, \tag{A.17}$$

$$\psi' = \psi(r)e^{-\mu t + in\theta}. \tag{A.18}$$

When this is inserted into the vorticity equations in the r- and θ-directions, it is seen that, given this base state, the only physically allowable two-dimensional perturbation has no azimuthal dependence, *i.e.* $n = 0$. From the vorticity equation in the z-direction, we obtain the equation for the perturbation quantities

$$L^0\omega + \mu\omega = \frac{6}{r}\left(1 - e^{-r^2/2}\right) + 6e^{-r^2/2}\omega, \tag{A.19}$$

$$L^0(\cdot) \equiv \frac{1}{r}\frac{d}{dr}\left(r\frac{d}{dr}(\cdot)\right) + \frac{1}{r}\frac{d}{dr}\left[r^2(\cdot)\right]. \tag{A.20}$$

Notice that this linear equation has no dependence on Reynolds number or the perturbation streamfunction. In order to tackle the problem numerically, we write A.19 as the general eigenvalue problem

$$\mathcal{L}(\omega) = -\mu\omega, \tag{A.21}$$

$$\mathcal{L}(\cdot) = L^0(\cdot) - \frac{6}{r}\left(1 - e^{-r^2/2}\right) - 6e^{-r^2/2}\omega. \tag{A.22}$$

A Galerkin approach is used to expand solutions in the orthogonal basis defined by the $R = 0$ vorticity eigenfunctions from Chapter 4,

$$\omega = \sum_{k=0}^{N-1} a_k\, \omega(r,k), \quad \omega(r,k) = e^{-r^2/2} L_k^{(0)}\left(r^2/2\right), \tag{A.23}$$

where the finite expansion is truncated at $N-1$ terms. Substitution of (A.23) into (A.19) results in a complex eigenvalue problem of the form

$$\mathbf{A}\vec{x} = -\mu\vec{x}, \tag{A.24}$$

where $\vec{x} = (a_0, a_1, ..., a_{N-1})^T$ and $\mathbf{A}$ is complex matrix of order $N \times N$ whose coefficients are found by using the orthogonality of the basis functions under the weighted inner product,

$$\langle u, v\rangle = \int_0^\infty u\bar{v}e^{r^2/2} r dr, \tag{A.25}$$

such that the coefficients of $\mathbf{A}$,

$$\mathbf{A}_{jk} = \frac{\langle \omega_j(r), \mathcal{L}\omega_k(r) \rangle}{\langle \omega_j(r), \omega_j(r) \rangle}, \tag{A.26}$$

follow from

$$\langle \omega_j(r), \omega_k(r) \rangle = \begin{cases} 0 & \text{if } k \neq j, \\ 1 & \text{if } k = j, \end{cases}, \tag{A.27}$$

$$\left\langle \omega_j(r), L^0\omega_k(r) \right\rangle = \begin{cases} 0 & \text{if } k \neq j, \\ 2j & \text{if } k = j, \end{cases}, \tag{A.28}$$

$$\left\langle \omega_j(r), \frac{1}{r}\omega_k(r) \right\rangle = \begin{cases} 0 & \text{if } j > k, \\ 1 & \text{if } j \leq k, \end{cases}, \tag{A.29}$$

$$\left\langle \omega_j(r), e^{-r^2/2}\omega_k(r) \right\rangle = -2^{-(j+k+1)}\frac{(j+k)!}{j!\,k!}, \tag{A.30}$$

$$\left\langle \omega_j(r), \frac{1}{r}e^{-r^2/2}\omega_k(r) \right\rangle = -2^{-(j+k+1)}a\left(j+1, k+1\right), \tag{A.31}$$

where

$$a(j+1, k+1) == \begin{cases} 2^{k+1} - 1 & \text{if } j = 0, \\ a(j, k+1) + a(j+1, k) & \text{if } j > 0. \end{cases} \tag{A.32}$$

A.2 Results

Numerical solutions to (A.19) are found using the QZ algorithm for values of N up to 100. We find a denumerable set of eigenfunctions and eigenvalues for $k = 0, 1, 2, ...,$ each corresponding to a different radial structure of the perturbation. A table of these eigenvalues appears in Table A.1. The eigenvalue close to zero has eigenfunction of the same form of the Sullivan vortex. This corresponds to a change in Reynolds number, so its stability is neutral, as expected. All other eigenvalues are positive, therefore the Sullivan vortex is shown to be stable to 2-D perturbations.

The stability of the Sullivan vortex to three-dimensional disturbances is a considerably complex problem, but a study of this should show at least one stable mode

as shown in Chapter 5. This stable mode corresponds to an in-plane displacement of vorticity by a three-dimensional perturbation, for which the vortex would be neutrally convected back to the origin.

Table A.1: Eigenvalues for two-dimensional perturbations to the Sullivan vortex

k	μ
0	-0.00001167
1	1.64283132
2	3.14848971
3	4.78395175
4	6.55784082
5	8.40255546
6	10.28554058
7	12.19251347
8	14.11613845
9	16.05221176
10	17.99818801
11	19.95244979
12	21.91389274
13	23.88167381
14	25.85507583
15	27.83342170
16	29.81603813
17	31.80222511
18	33.79124069

Bibliography

[1] M. Abramowicz and I. A. Stegun. *Handbook of Mathematical Functions.* Nat. Bur. Standards; Dover, 1972.

[2] W. T. Ashurst, A. R. Kerstein, R. M. Kerr, and C. H. Gibson. Alignment of vorticity and scalar gradient with strain in simulated Navier-Stokes turbulence. *Phys. Fluids*, 30:2343–2353, 1987.

[3] J. D. Buntine and D. I. Pullin. Merger and cancellation of strained vortices. *J. Fluid Mech.*, 205:263–295, 1989.

[4] J. M. Burgers. A mathematical model illustrating the theory of turbulence. *Advances in Applied Mechanics*, 1:171–199, 1948.

[5] S. Douady, Y. Couder, and M. E. Brachet. Direct observation of the intermittency of intense vorticity filaments in turbulence. *Physical Review Letters*, 67(8):983–986, 1991.

[6] C. duP. Donaldson and R. D. Sullivan. Behavior of solutions of the Navier-Stokes equations for a complete class of three-dimensional viscous vortices. In D. M. Mason et al., editor, *Proceedings of the 1960 Heat Transfer and Fluid Mechanics Institute*, pages 16–30. Stanford, U. P., 1960.

[7] J. Jiménez, H. K. Moffatt, and C. Vasco. The structure of vortices in freely decaying two-dimensional turbulence. *J. Fluid Mech.*, Submitted June 23, 1995.

[8] J. Jiménez and A. A. Wray. Columnar vortices in isotropic turbulence. *Meccanica*, 29:453–464, 1994.

[9] J. Jiménez, A. A. Wray, P. G. Saffman, and R. S. Rogallo. The structure of intense vorticity in isotropic turbulence. *J. Fluid Mech.*, 255:65–90, 1993.

[10] R. M. Kerr. Higher order derivative correlation and the alignment of small-scale structures in isotropic turbulence. *J. Fluid Mech.*, 153:31–58, 1985.

[11] S. Kida and K. Ohkitani. Spatiotemporal intermittency and instability of a forced turbulence. *Phys. Fluids A*, 4(5):1018–1027, 1992.

[12] S. Leibovich and P. Holmes. Global stability of Burgers vortex. *Phys. Fluids*, 24(3):548–549, 1981.

[13] S. J. Lin and G. M. Corcos. The mixing layer: deterministic models of a turbulent flow. part 3. the effect of plane strain on the dynamics of streamwise vortices. *J. Fluid Mech.*, 141:139–178, 1984.

[14] H. K. Moffatt, S. Kida, and K. Ohkitani. Stretched vortices - the sinews of turbulence; large-Reynolds-number asymptotics. *J. Fluid Mech.*, 259:241–264, 1994.

[15] D. I. Pullin and P. G. Saffman. Calculation of velocity structure functions for vortex models of isotropic turbulence. *Phys. Fluids*, 8(11):3072–3084, 1996.

[16] G. R. Reutsch and M. R. Maxey. Small scale features of vorticity and passive scalar fields in homogeneous isotropic turbulence. *Phys. Fluids A*, 3(6):1587–1597, 1991.

[17] A. C. Robinson and P. G. Saffman. Stability and structure of stretched vortices. *Studies in Applied Mathematics*, 70:163–181, 1984.

[18] Y. Saad. *Numerical Methods for Large Eigenvalue Problems.* Manchester University Press, 1992.

[19] Z.-S. She, E. Jackson, and S. A. Orszag. Structure and dynamics of homogeneous turbulence - models and simulations. *Proc. Roy. Soc.*, 434:101–124, 1991.

[20] G. I. Taylor. Production and dissipation of vorticity in a turbulent fluid. *Proc. Roy. Soc. London Ser. A*, 164:15–23, 1938.

[21] A. A. Townsend. On the fine-scale structure of turbulence. *Proc. Roy. Soc. London Ser. A*, 208:534–542, 1938.

[22] A. Vincent and M. Meneguzzi. The spatial and statistical properties of homogeneous turbulence. *J. Fluid Mech.*, 225:1–20, 1991.